DOE/ET-53088-639 IFSR #639

L-H Confinement Mode Dynamics in Three-Dimensional State Space

H. SUGAMA
National Institute for Fusion Science
Nagoya 464-01, Japan
and
W. HORTON
Institute for Fusion Studies
The University of Texas at Austin
Austin, Texas 78712

July 1994
(Revised)

L-H confinement mode dynamics in three-dimensional state space

H. Sugama

National Institute for Fusion Science, Nagoya 464-01, Japan

and

W. Horton

Institute for Fusion Studies, The University of Texas at Austin

Austin, Texas 78712

A dynamical model for the low-high (L-H) confinement mode transitions consisting of three ordinary differential equations (3-ODE model) for the essential state variables is proposed. The model is derived from the energy balance equations for the resistive pressure-gradient-driven turbulence and describes temporal evolutions of three characteristic variables (u, k, f), the potential energy contained in the pressure gradient, the turbulent kinetic energy and the shear flow energy. The energy input to the peripheral plasma region is included as an external control parameter in the model. The model equations have stationary solutions corresponding to the L and H modes. The L to H and H to L transitions are obtained by varying the energy input parameter. The type of L-H transition, whether like a first-order or second-order transition, is shown to be determined by the shear flow damping. At a higher level of the energy input parameter the H mode stationary solution becomes unstable and bifurcates to a limit cycle which shows periodic oscillations characteristic of the H localized mode (ELM) confinement state.

To appear in *Plasma Physics and Controlled Fusion*

I. Introduction

In order to explain the mechanism of the L-H transitions observed in many tokamaks and in some stellarators, various theoretical models have been proposed in recent years.[1-7] The key points that such models attempt to describe are how the radial electric field or the poloidal shear flow suppresses the turbulence and anomalous transport, and how the electric field or the shear flow is produced. In our previous work,[7] the spontaneous shear flow generation and the resultant transport reduction similar to the L-H transition are shown in a single-helicity nonlinear simulation of the resistive g modes.[8-12] The simulations and supporting theory suggest that the shear flow generation is triggered by the decrease of the collisional shear flow damping due to the increase of the temperature.

Shaing *et al.*[3] and Hassam *et al.*[4] also argue in their L-H transition models that the bifurcation of the poloidal flow is caused by the decrease of the poloidal flow damping. However, the poloidal rotation is driven by the torque due to the ion orbit loss in the theory of Shaing *et al.* and due to the poloidal asymmetric radial diffusion in the model of Hassam *et al.*, while our simulation showed that the Reynolds stress directly generates the shear flow.

The plasma mass flow generation by the divergence of the Reynolds stress arises from the nonlinear convective derivative in the mass acceleration term. This mechanism for flow generation is based on the self-consistent hydrodynamics for the interaction between the plasma turbulence and the background mass flow and has been supported by several other theoretical works.[13-17] In the L-H transition model presented in the present work, the Reynolds stress is considered to be the cause of the shear flow generation.

Diamond *et al.*[6] have also presented an L-H transition model which describes the temporal behavior of the turbulence fluctuation and the shear flow although the pressure gradient is fixed as an external parameter. In actual experiments, the pressure gradient also changes at

the L-H transition according to the change in the transport. Therefore, our model contains the pressure gradient as a basic state variable as well as the fluctuation energy density and the mean flow kinetic energy density. Thus, the state of the system is specified by these three dynamical variables which interact through the hydrodynamic nonlinearities. Our model consists of the three ordinary differential equations (3-ODE model) which govern the temporal evolution of the three system state variables. The model reduces to the 2-ODE model of Diamond *et al.*[6] if the pressure gradient variable is fixed. In the Diamond *et al.* model, the stable H mode solution appears when some criterion is satisfied by the external parameter. There, the L-H transition is considered as a second-order phase transition: the magnitudes of the fluctuation and the flow are continuously changed at the critical point of the transition. In contrast, most of other L-H transition models have claimed that the L-H transition should be like a first-order phase transition where the fluctuation and the flow are changed discontinuously at the transition and the hysteresis property appears.

In our 3-ODE model, the energy input to the peripheral plasma region is regarded as an external control parameter. It will be shown that the type of the L-H transition is like either a first-order or a second-order phase transition depending on the form of the collisional shear flow damping. In addition, we show that under certain conditions the present model predicts the transition from the H mode to a time dependent state with relaxation oscillations characteristic of the edge localized modes (ELM) observed in sufficiently high-beta H mode plasmas. In order to explain the edge localized modes (ELM), Leboeuf *et al.* proposed another 2-ODE model which has the same form as the Volterra-Lotka equations.[18] Our 3-ODE model has the ELM behavior occurring as a subset of the parameter region in which the H mode stationary solution becomes unstable and bifurcates to a limit cycle which shows periodic relaxation oscillations like those observed in the ELM state.

This work is organized as follows. In Sec. II, our three-state variables are defined, and the 3-ODE model is derived from the energy balance equations of the resistive pressure-

gradient-driven turbulence by modeling the energy transfer and dissipation terms. There we also explain the L and H mode stationary solutions and the condition for the existence of the H mode. In Sec. III, the linear stabilities of the L and H mode stationary solutions are examined and the criterion for the unstable H mode (or occurrence of the ELM) is derived. In Sec. IV, numerical solutions of our model equations are given. We show the temporal behavior of the pressure gradient, turbulence and shear flow energy for various values of the external thermal power input parameter giving examples of the L and H modes and the ELM-like limit cycle. In Sec. IV numerical solutions are shown for the case where the power input is temporally varied to show the difference between the first-order and second-order phase transitions. Finally, the conclusions and discussion are given in Sec. V.

II. Model Equations

Basic variables for our dynamical model of L-H transtions are the turbulent kinetic energy K, the background shear flow kinetic energy F, and the potential energy related to the pressure profile U, which are defined by

$$K \equiv \frac{1}{\delta}\int_{-\delta}^{0} dx \, \frac{1}{2}\left\langle \tilde{v}^2 \right\rangle \ , \quad F \equiv \frac{1}{\delta}\int_{-\delta}^{0} dx \, \frac{1}{2} v_0^2 \ , \quad U \equiv \frac{1}{\delta}\int_{-\delta}^{0} dx \, \frac{(-x)}{L_c}\frac{P_0}{n_0 m_i} \tag{1}$$

respectively, where we define the peripheral region by $-\delta \le x \le 0$. Here, $x = 0$ corresponds to the plasma surface, or the last closed flux surface, and δ represents the radial width of the shear flow layer, in which the resistive pressure gradient driven turbulence is a dominant cause of the anomalous transport and an energy source of the shear flow generation. The angle bracket $\langle \cdot \rangle$ denotes the average over the (y, z)-plane (or the magnetic surface). The velocity and the pressure are divided into the x-dependent average parts and the fluctuating parts as $\mathbf{v} = \mathbf{v}_0(x) + \tilde{\mathbf{v}}$ and $p = p_0(x) + \tilde{p}$, respectively. The average mass density is denoted by $n_0\, m_i$. The unfavorable average magnetic curvature is represented by $1/L_c = d\Omega/dx$[7,19] and is assumed to be constant. The curvature reduces to $2/R$ for modes localized to the

outside of a small aspect ratio tokamak with major radius R.

From the reduced resistive MHD equations (1) and (2) in Ref.7 with the electrostatic approximation in the sheared slab geometry, we obtain the following energy balance equations

$$\frac{dU}{dt} = P_U - P_K \tag{2}$$

$$\frac{dK}{dt} = P_K - P_F - \epsilon_K \tag{3}$$

$$\frac{dF}{dt} = P_F - \epsilon_F \tag{4}$$

where the production and dissipation terms in the right-hand sides are given by

$$P_U \equiv \frac{\langle \widetilde{p}\widetilde{v}_x \rangle |_{x=-\delta}}{L_C n_0 m_i} \tag{5}$$

$$P_K \equiv \frac{1}{\delta}\int_{-\delta}^{0} dx \frac{\langle \widetilde{p}\widetilde{v}_x \rangle}{L_C n_0 m_i} \tag{6}$$

$$P_F \equiv \frac{1}{\delta}\int_{-\delta}^{0} dx \langle \widetilde{v}_x \widetilde{v}_y \rangle \frac{dv_0}{dx} \tag{7}$$

$$\epsilon_K \equiv \frac{1}{\delta}\int_{-\delta}^{0} dx \left\{ \mu \left\langle \left(\frac{\partial \widetilde{v}_i}{\partial x_j} \right)^2 \right\rangle + \frac{\eta}{n_0 m_i} \left\langle \widetilde{J}_\parallel^2 \right\rangle \right\} \tag{8}$$

$$\epsilon_F \equiv \frac{1}{\delta}\int_{-\delta}^{0} dx \mu \left(\frac{dv_0}{dx} \right)^2 . \tag{9}$$

Here μ denotes the (kinematic) viscosity, η the resistivity and $\widetilde{J}_\parallel = -\eta^{-1}\nabla_\parallel \phi$ the parallel current. The electrostatic potential ϕ gives the velocity as $\mathbf{v} = -(c/B_0)\nabla\phi \times \hat{\mathbf{z}}$ in the reduced MHD model. In the temporal evolution equation for U, we have neglected the collisional dissipation term by assuming that the turbulent thermal transport is much larger than the collisional one. In order to solve Eqs. (2)–(4), the production and dissipation terms (5)–(9) need to be expressed in terms of U, K and F. Before proceeding to this closure problem, some remark on these terms should be given here. The potential energy production P_U is given by the energy input to the peripheral region through the inner boundary at $x = -\delta$, the

turbulent energy production P_K is expressed in terms of the pressure transport multiplied by the unfavorable curvature, which is originally from the potential energy, and the background flow production is represented by the product of the Reynolds stress and the flow shear, which comes from the turbulent kinetic energy. As for the dissipation terms, ϵ_K stands for the viscous and Joule dissipations of the fluctuation, and ϵ_F the viscous dissipation of the average flow. In equilibria, we obtain $P_U = P_K = \epsilon_K + \epsilon_F$ and $P_F = \epsilon_F$. From the definitions, we also find that $P_F = \epsilon_F = 0$ in the case of no shear flow (since $dv_0/dx = 0$) as in the L mode phase. When P_F is positive, the stationary value of the turbulent energy dissipation $\epsilon_K = P_U - P_F$ becomes smaller than in the no shear flow case, which implies the reduction of the turbulence level as observed in the H mode phase.

Now let us consider the closure problem. The time scale τ_c in the g or ballooning mode turbulence is given by $\tau_c \sim [t] \equiv (L_c n_0 m_i/|dP_0/dx|)^{1/2}$. Approximating the background pressure profile as $P_0(x) \simeq P_0(x=0) + x dP_0/dx$, we have

$$U \simeq \frac{1}{3}\frac{\delta^2}{L_c n_0 m_i}\left|\frac{dP_0}{dx}\right| + \frac{1}{2}\frac{\delta P_0(x=0)}{L_c n_0 m_i} \tag{10}$$

where we assumed that $dP_0/dx < 0$ and $n_0 \simeq$ const. Hereafter U is redefined by the pressure gradient term in Eq. (10) as $U \equiv \delta^2|dP_0/dx|/(3L_c n_0 m_i)$ assuming that the pressure at the outer boundary $P_0(x=0) =$ const. Then we obtain

$$\tau_c \sim \delta U^{-1/2} \tag{11}$$

Estimating the anomalous pressure diffusivity as $D \sim \tau_c K$, we have

$$P_K \sim \frac{D|dP_0/dx|}{L_c n_0 m_i} \sim \tau_c^{-1} K \sim \delta^{-1} U^{1/2} K\ . \tag{12}$$

In the same way as in the background pressure profile, we approximate the background flow profile as $v_0(x) \simeq v_0(x=0) + x dv_0/dx$. Then F is given by

$$F \simeq \frac{1}{2}(\overline{v}_0)^2 + \frac{1}{24}\delta^2\left(\frac{dv_0}{dx}\right)^2 \tag{13}$$

where $\overline{v}_0 \equiv \delta^{-1}\int_{-\delta}^{0} v_0(x)dx$ denotes the volume-averaged poloidal flow. Hereafter we also redefine F as $F \equiv \delta^2(dv_0/dx)^2/24$ since the volume-averaged velocity $\overline{v}_0$ is not accelerated by the divergence of the Reynolds stress $-d\left\langle \tilde{v}_x\tilde{v}_y\right\rangle /dx$. The Reynolds stress is approximated by $\left\langle \tilde{v}_x\tilde{v}_y\right\rangle \sim \tau_c(dv_0/dx)K$. We obtain

$$P_F \sim \tau_c K(dv_0/dx)^2 \sim \delta^{-1}U^{-1/2}FK\ . \tag{14}$$

Assuming that the Joule dissipation is dominant in (8), the turbulent energy dissipation can be written[20] as

$$\epsilon_K \sim D_L^{-1}K^2 \tag{15}$$

where $D_L = D_L(U)$ is, as seen later, the L mode anomalous diffusivity and a function of U through its dependence on the background temperature. This form of the turbulent energy dissipation $\epsilon_K \propto K^2$ is the same as in the Diamond's 2-ODE model. Finally the background flow energy dissipation is written as

$$\epsilon_F \sim \mu\delta^{-2}F \tag{16}$$

where the ion viscosity $\mu = \mu(U)$ is also given as a function of U due to the temperature dependence of the viscosity. Thus a closed set of the equations for U, K and F are obtained as follows

$$\frac{dU}{dt} = P_U - C_K\delta^{-1}U^{1/2}K \tag{17}$$

$$\frac{dK}{dt} = C_K\delta^{-1}U^{1/2}K - C_F\delta^{-1}U^{-1/2}FK - C'_K D_L^{-1}K^2 \tag{18}$$

$$\frac{dF}{dt} = C_F\delta^{-1}U^{-1/2}FK - C'_F\delta^{-2}\mu F \tag{19}$$

where the potential energy U input power $P_U(>0)$ is regarded as an external parameter and C's are nondimensional numerical constants.

The constants C's may be estimated either through comparisons of the solutions of Eqs. (17)–(19) with numerical simulations or empirically from modelling time series obtained for L-H and ELM dynamics in tokamaks.

Stationary solutions of Eqs. (17)–(19) can be easily obtained. The L mode solution in the L mode case is given by

$$F = 0 \ , \quad K = \delta^{-1} C_K C_K'^{-1} D_L(U_L) U_L^{1/2} \quad U = U_L \tag{20}$$

where $U_L = U_L(P_U)$ is a function of P_U given by the solution of

$$C_K C_K'^{-1} D_L(U_L) U_L = C_K^{-1} \delta^2 P_U \ . \tag{21}$$

In this case, the anomalous pressure diffusivity $D \sim \tau_c K$ is written as

$$D = C_P \delta U^{-1/2} K = C_P C_K C_K'^{-1} D_L(U_L) \tag{22}$$

which confirms the previous statement that D_L agrees with the L mode diffusivity except for the nondimensional numerical factor.

Another stationary solution, i.e., the H mode stationary solution is given by

$$F = C_K' C_F^{-1} U_H D_L^{-1}(U_H) [C_K C_K'^{-1} D_L(U_H) - C_F^{-1} C_F' \mu(U_H)]$$

$$K = \delta^{-1} C_F^{-1} C_F' \mu(U_H) U_H^{1/2}$$

$$U = U_H \ . \tag{23}$$

In this stationary state the fluctuation level is controlled by the viscous damping of the mean shear flow. The H mode solution exists only when

$$C_K C_K'^{-1} D_L(U_H) > C_F^{-1} C_F' \mu(U_H) \ . \tag{24}$$

Condition (24) requires that the viscous drag be sufficiently weak compared to the thermal diffusivity, $\mu / D_L <$ const, for the onset of the H mode. Essentially, this requires that the edge ion temperature be sufficiently high.

From Eqs. (20) and (23) we see that when the H mode condition (24) is satisfied the turbulence level K is decreased. Here $U_H = U_H(P_U)$ is a function of P_U given by the solution of

$$C_F^{-1} C_F' \mu(U_H) U_H = C_K^{-1} \delta^2 P_U \ . \tag{25}$$

The anomalous pressure diffusivity in the H mode is written as

$$D = C_P \delta U^{-1/2} K = C_P C_F^{-1} C_F' \mu(U_H) \ . \tag{26}$$

From Eqs. (22) and (26), we obtain the ratio of the H mode to L mode pressure diffusivity for $P_U > P_c$, which is given by

$$\frac{D(H)}{D(L)} = \frac{C_F^{-1} C_F' \mu(U_H)}{C_K C_K'^{-1} D_L(U_L)} = \frac{U_L}{U_H} < 1 \tag{27}$$

where Eqs. (21) and (25) are used.

Now let us define (P_{c1}, U_{c1}) by the solution of

$$C_K^{-1} \delta^2 P_{c1} = C_K C_K'^{-1} U_{c1} D_L(U_{c1}) = C_F^{-1} C_F' U_{c1} \mu(U_{c1}) \ . \tag{28}$$

We assume that Eq. (28) has only a unique solution (P_{c1}, U_{c1}) and consider the two cases where $UD_L(U)$ and $U\mu(U)$ are functions of U as shown schematically in Figs. 1(a) and (b).

The condition for the existence of the H mode stationary solution is given by $P_U > P_{c1}$ in the case of Fig. 1(b). In the case of Fig. 1(a), the H mode solution exists for $P_U > P_{c2}$ where $C_K^{-1} \delta^2 P_{c2}$ denotes the minimum value of $C_F^{-1} C_F' U_{c1} \mu(U)$ at $U = U_{c2} > U_{c1}$ as shown in Fig. 1(a). In the latter case, Eq. (25) has the two solutions for $P_{c2} < P_U < P_{c1}$, which are denoted by U_{H-} and $U_{H+} (> U_{H-})$. As seen in the next section, U_{H-} is unstable and U_{H+} corresponds to the real H mode.

Before ending this section, we introduce the following normalized variables, functions and

parameters

$$u = U/U_{c1}, \quad k = K/U_{c1}, \quad f = F/U_{c1}, \quad \tau = C_K \delta^{-1} U_{c1}^{1/2} t$$

$$d(u) = C_K C_K'^{-1} \delta^{-1} U_{c1}^{-1/2} D_L(U) \ , \quad m(u) = C_F^{-1} C_F' \delta^{-1} U_{c1}^{-1/2} \mu(U) \tag{29}$$

$$q = C_K^{-1} \delta U_{c1}^{-3/2} P_U \ , \quad c = C_F/C_K$$

in terms of which, Eqs. (17)–(19) are rewritten as

$$\frac{du}{d\tau} = q - u^{1/2} k \tag{30}$$

$$\frac{dk}{d\tau} = u^{1/2} k - c u^{-1/2} f k - d^{-1}(u) k^2 \tag{31}$$

$$\frac{df}{d\tau} = c u^{-1/2} f k - c m(u) f \ . \tag{32}$$

The L and H mode stationary points are give by the normalized variables as

$$(u_L, k_L, f_L) \ , \quad (u_H, k_H, f_H) \tag{33}$$

respectively, where

$$\begin{aligned} k_L &= u_L^{1/2} d(u_L) \ , \quad f_L = 0 \\ k_H &= u_H^{1/2} m(u_H) \ , f_H = c^{-1} u_H d^{-1}(u_H)(d(u_H) - m(u_H)) \end{aligned} \tag{34}$$

and u_L and u_H are functions of the external parameter q defined by

$$u_L d(u_L) = u_H m(u_H) = q \ . \tag{35}$$

The condition for the existence of the H mode stationary solution is written as

$$d(u_H) > m(u_H) \tag{36}$$

The critical value q_{c1} is given by solving

$$u_{c1} d(u_{c1}) = u_{c1} m(u_{c1}) = q_{c1}. \tag{37}$$

where $u_{c1} \equiv 1$ from the normalization in Eq. (29). In the case of Fig. 1(b), the condition (36) is equivalent to $q > q_{c1}$. In the case of Fig. 1(a), the H mode solution exists for $q > q_{c2}$ where q_{c2} is the minimum value of $um(u)$ at $u = u_{c2}(> u_{c1} \equiv 1)$. In this case, for $q_{c2} < q < q_{c1}$, the equation $um(u) = q$ has two solutions u_{H-} and $u_{H+}(> u_{H-})$ where u_{H-} is unstable and u_{H+} corresponds to the real H mode.

III. Linear Stability of the L and H States

In this section, we examine linear stabilities of the L and H mode stationary solutions obtained in the previous section.

Putting $(u, k, f) = (u_L, k_L, f_L) + (\tilde{u}, \tilde{k}, \tilde{f})$ and linearizing Eqs. (30)–(32) around the L mode stationary solution, we obtain the following equations

$$\frac{d}{d\tau}\begin{pmatrix}\tilde{u}\\ \tilde{k}\\ \tilde{f}\end{pmatrix} = M_L \begin{pmatrix}\tilde{u}\\ \tilde{k}\\ \tilde{f}\end{pmatrix} \tag{38}$$

where M_L is a matrix defined by

$$M_L = \begin{pmatrix} -\frac{1}{2}d_L & -u_L^{1/2} & 0 \\ \frac{1}{2}d_L + u_L d'_L & -u_L^{1/2} & -cd_L \\ 0 & 0 & c(d_L - m_L) \end{pmatrix} \tag{39}$$

Here $d_L \equiv d(u_L)$, $m_L \equiv m(u_L)$, $d'_L \equiv d'(u_L)$ and $'$ denotes the derivative with respect to u. The eigenvalues of M_L are easily obtained as

$$\lambda_{L1} \equiv c(d_L - m_L)\ , \qquad \lambda_{L+}\ , \qquad \lambda_{L-} \tag{40}$$

where λ_{L+} and λ_{L-} are the solutions of the quadratic equations

$$\lambda^2 + \left(\frac{1}{2}d_L + u_L^{1/2}\right)\lambda + u_L^{1/2}(u_L d_L)' = 0\ . \tag{41}$$

We find that Re $\lambda_{L+} < 0$ and Re $\lambda_{L-} < 0$ since $(ud)' > 0$ is assumed as seen in Figs. 1(a) and (b). The eigenvectors corresponding to λ_{L+} and λ_{L-} are both tangential to the (u, k)-plane

defined by $f = 0$ and the L mode solution $(u_L, k_L, 0)$ is a sink for the orbits on this plane. The L mode solution is unstable if and only if $d_L > m_L$ which is equivalent to the condition $q > q_{c1}$.

Next, in the similar way as above, putting $(u, k, f) = (u_H, k_H, f_H) + (\tilde{u}, \tilde{k}, \tilde{f})$ and linearizing Eqs. (30)–(32) around the H mode solution yield the following equations

$$\frac{d}{d\tau}\begin{pmatrix}\tilde{u}\\ \tilde{k}\\ \tilde{f}\end{pmatrix} = M_H \begin{pmatrix}\tilde{u}\\ \tilde{k}\\ \tilde{f}\end{pmatrix} \tag{42}$$

with

$$M_H = \begin{pmatrix} -\frac{1}{2}m_H & -u_H^{1/2} & 0 \\ m_H - \frac{1}{2}\, m_H^2/d_H + u_H m_H^2\, d_H'/d_H^2 & -u_H^{1/2}\, m_H/d_H & -cm_H \\ -(1 - m_H/d_H)\left(\frac{1}{2}\, m_H + u_H\, m_H'\right) & u_H^{1/2}(1 - m_H/d_H) & 0 \end{pmatrix} \tag{43}$$

where $d_H \equiv d(u_H)$, $m_H \equiv m(u_H)$ and $m_H' \equiv m'(u_H)$. The eigenvalues of M_H are given by the solutions of

$$\lambda^3 + A\,\lambda^2 + B\,\lambda + C = 0 \tag{44}$$

where

$$A = m_H\left(\frac{1}{2} + \frac{u_H^{1/2}}{d_H}\right)$$

$$B = u_H^{1/2} m_H((1+c)(1 - m_H/d_H) + m_H(u_H d_H)'/d_H^2)$$

$$C = c u_H^{1/2} m_H (u_H m_H)'(1 - m_H/d_H)\ . \tag{45}$$

Here we consider the case in which the condition for the existence of the H mode solution $d_H > m_H$ is satisfied. It is found that both A and B are positive. In the case of $u_H = u_{H-}$ in Fig. 1(a) where $q_{c2} < q < q_{c1}$, we obtain $C < 0$ since $(um)' < 0$ for $u_{c1} < u < u_{c2}$. Then the stationary point (u_{H-}, k_{H-}, f_{H-}) is unstable since Eq. (44) has one real and positive solution for $C < 0$. For the H mode stationary point in Fig. 1(b) and for that at $u > u_{c2}$ in Fig. 1(a), we have $C > 0$ and therefore at least one real and negative solution of Eq. (44).

In these cases where $C > 0$, other two solutions of Eq. (44) are both real and negative or a pair of complex conjugate values since both A and B are positive. Thus the marginal stability of the H mode solution except for (u_{H-}, k_{H-}, f_{H-}) occurs when $C = AB$ which implies that Eq. (44) has a pair of pure imaginary solutions. Then these H mode solutions become unstable when $C > AB$ which is rewritten as

$$\frac{(u_H m_H)'}{m_H} > \left(1 + c^{-1} + c^{-1} \frac{m_H/d_H}{1 - m_H/d_H} \frac{(u_H d_H)'}{d_H}\right) \left(\frac{1}{2} + \frac{u_H^{1/2}}{d_H}\right) . \tag{46}$$

This criterion for the instability of the H mode depends on the values of q (through $u_H = u_H(q)$), c as well as the functional forms of $d(u)$ and $m(u)$. As shown by the numerical examples in the next section, there appears a Hopf-bifurcation from the stable H mode solution to the limit cycle around the unstable H mode solution just when the criterion (46) is satisfied.

Technically, the language of bifurcation theory should be used to describe the transitions between the sequence of states rather than the terms "first and second order phase transitions." Traditionally, the terms "phase transitions" apply to the statistical behavior of the many-body system. While not established, the idea here is that the statistical physics does apply to the underlying infinite degree of freedom partial differential equations upon which the Eqs. (1)–(9) and their closure given in Eqs. (17)–(19) are based. It requires further investigation to establish the degree of correspondence between the two systems.

IV. Numerical Modeling

Here we explore the properties of Eqs. (30)–(32) for two models of the function $d(u)$ and $m(u)$ based on neoclassical viscosity and turbulent viscosity. Simulations by Hamaguchi[9] and scaling theory by Connor[21] show that the anomalous diffusivity is proportional to the pressure gradient. Thus, we take

$$d(u) = u \tag{47}$$

in all the numerical calculations reported here. The unit coefficient is not a direct result from the normalization (29). From Eqs. (10) and (29), we have $D_L \sim \delta^2 v_{Ti}/\sqrt{L_p L_c}\cdot d(u)$ with the scale length L_p of the pressure gradient. Thus the unit coefficient in Eq. (47) corresponds to $D_L(U_{c1}) \sim \delta^2 v_{Ti}/\sqrt{L_p L_c}$ ($\leq 10\,\mathrm{m}^2/\mathrm{s}$ if $\delta \sim 1\,\mathrm{cm}$, $\sqrt{L_p L_c} \sim 1\,\mathrm{m}$ and $T \leq 100\,\mathrm{eV}$). In the high pressure gradient limit $u \gg 1$ the anomalous viscosity from small scale turbulence giving $m(u) = c_\mu u$ where the positive constant c_μ is small [$\sim .01$ to $.05$].

For smaller pressure gradients the neoclassical viscosity[22]

$$\mu_{\mathrm{nc}} = \frac{Rqv_{Ti}\nu_{*i}}{(1+\nu_{*i})(1+\epsilon^{3/2}\nu_{*i})}$$

where $\nu_{*i} = Rq\nu_i/v_{Ti}\epsilon^{3/2}$ and $\epsilon = r/R$ gives the damping of the mean shear flow through $dF/dt \cong -(3\mu_{\mathrm{nc}}/R^2(1+2q^2))F$ which has a strong ion temperature dependence varying as $T_i^{-3/2}$ for $\nu_{*i} \ll 1$ and $T_i^{1/2}$ for $1 \ll \nu_{*i} \ll \epsilon^{-3/2}$. Here we model this dependence by taking u proportional to T_i and introduce $m(u) \approx u^{-3/2}$ for model A as in the banana regime and for model B the transitional dependence of $m(u) \approx u^{-1}$ for low u.

Thus, for the numerical studies we take

Case A
($\nu_{*i} \ll 1$)
$$m(u) = u^{-3/2}(0.95 + 0.05u^{5/2})$$

Case B
($\nu_{*i} \sim 1$)
$$m(u) = u^{-1}(0.97 + 0.03u^2)\ . \tag{48}$$

Figures 2(a) and (b) show $ud(u)$ and $um(u)$ from Eq. (48) for Case A and Case B, respectively. We can see that Case A and Case B correspond to the cases in Figs. 1(a) and (b), respectively. We put $c = 5$ for which we can satisfy the H mode instability criterion (46).

Case A (banana regime $\nu_{*i} \ll 1$)

By the normalization in Eq. (29), we have $u_{c1} \equiv 1$. From Eqs. (37), (46), (47) and (48), we obtain $q_{c1} = 1$, $u^*_{c1} = 3.01$, $u_{c2} = 1.86$, $u^*_{c2} = 0.93$, $q_{c2} = 0.87$, $u_{c3} = 4.40$ and $q_{c3} = 1.42$,

which are shown in Fig. 2(a). Here (q_{c3}, u_{c3}) denotes the critical point for the bifurcation of the H mode into the limit cycle associated with ELM state. The solid and dashed curves in Fig. 2 correspond to the stable and unstable stationary solutions, respectively.

For $q < q_{c2}$, there exists only one stationary solution, i.e., the stable L mode solution. Figures 3(a), (b), and (c) show the numerical solution of Eqs. (30)–(32) as the trajectory in the (u, k, f) phase space, its projection onto the (k, f)-plane and the temporal dependence of (u, k, f), respectively, where the external parameter $q = 0.8$ and the initial condition $(u, k, f)_{\tau=0} = (0.3, 0.2, 0.1)$ are used. Here we see that the trajectory is approaching the stable L mode solution $(u_L, k_L, f_L) = (0.89, 0.85, 0)$.

For $q_{c2} < q < q_{c1}$, the L mode stationary solution remains stable while there appears one stable H mode solution and another unstable stationary solution. Figures 4(a)–(d) show the numerical solutions for $q = 0.9$ with two different initial conditions $(u, k, f)_{\tau=0} = (1.5, 0.2, 0.08)$ and $(u, k, f)_{\tau=0} = (1.5, 0.2, 0.1)$. Here, both the solutions firstly are close to each other along the stable manifold shrinking to the unstable stationary point $(u_{H-}, k_{H-}, f_{H-}) = (1.41, 0.76, 0.15)$ before reaching the unstable manifolds expanding from the point. (The linearized matrix around this unstable point has one positive real eigenvalue and a pair of complex-conjugate eigenvalues with negative real parts.) Then the two solutions deviate from each other : the one starting from $(u, k, f)_{\tau=0} = (1.5, 0.2, 0.08)$ goes to the L mode stable point $(u_L, k_L, f_L) = (0.95, 0.92, 0)$ and the other starting from $(u, k, f)_{\tau=0} = (1.5, 0.2, 0.1)$ to the H mode stable point $(u_{H+}, k_{H+}, f_{H+}) = (2.39, 0.58, 0.40)$.

For $q_{c1} < q < q_{c3}$, the L mode stationary solution is unstable and the stable H mode solution appears. Figures 5(a)–(c) show the numerical solution for $q = 1.05$ and $(u, k, f)_{\tau=0} = (0.3, 0.2, 0.1)$. Here the trajectory starting from $(u, k, f)_{\tau=0} = (0.3, 0.2, 0.1)$ first approaches to the L mode solution $(u_L, k_L, f_L) = (1.02, 1.04, 0)$ tangentially to the (k, f)-plane at $f = 0$ and next leave it at angle to the (k, f)-plane and finally goes to the H mode solution $(u_H, k_H, f_H) = (3.23, 0.58, 0.58)$. For $q > q_{c3}$, the L mode solution remains unstable and the

H mode solution also becomes unstable. Figures 6(a)–(d) show the numerical solution for $q = 1.6$ and $(u, k, f)_{\tau=0} = (0.3, 0.2, 0.1)$. Here we find that the trajectory finally approaches to a limit cycle existing around the H mode solution $(u_H, k_H, f_H) = (4.83, 0.73, 0.90)$. Thus we obtain the Hopf-bifurcation at $q = q_{c3} = 1.42$.

Let us regard a value of u for the stable stationary solution as an 'order parameter' in our system and consider it as a function $u = u(q)$ of the external parameter q. Due to the parameter region $q_{c2} < q < q_{c1}$ where the two stable stationary solutions exist, we obtain the hysteresis curve of the order paramater $u = u(q)$ as shown by arrows in Fig. 2(a). At the critical points $q = q_{c1}$ and $q = q_{c2}$ of the L to H and H to L transitions, the order parameter u changes discontinuously with respect to q as $u_{c1} \to u^*_{c1}$ and $u_{c2} \to u^*_{c2}$. Thus the L-H transition in Case A is like a first-order phase transition.

Since the L-H transition is achieved experimentally by adding additional plasma heating, it is interesting to consider a ramped up and down time profile for the control parameter q. In Fig. 7, we find the results where the external parameter is temporally varied. Figure 7(a) shows the external parameter $q = q(\tau)$ as a function of time. The temporal dependence of (u, k, f), its trajectories in the (u, k, f)-space and in the (k, f)-plane are shown in Figs. 7(b), (c), and (d), respectively. The hysteresis nature can be clearly seen in that the L to H transition occurs when $q > q_{c1} = 1$ while the H to L transition occurs when $q < q_{c2} = 0.87$. We can also see that, while $q > q_{c3} = 1.42$, the ELM-like instability grows approaching to the periodic oscillation represented by the limit cycle.

Case B (transitional regime $\nu_{*i} \sim 1$)

Here, we have $u_{c1} \equiv 1$, $q_{c1} = 1$, $u_{c3} = 6.28$ and $q_{c3} = 2.15$, which are shown in Fig. 2(b).

For $q < q_{c1}$, there exist only one stationary solution, i.e., the stable L mode solution. In this case we find the numerical solution of Eqs. (30)–(32) similar to that for $q < q_{c2}$ in Case A as shown in Fig. 3. For $q_{c1} < q < q_{c3}$ and $q > q_{c3}$, the stability of the L

and H stationary solutions and the behavior of the trajectories are similar to those in the corresponding parameter regions in Case A as shown in Figs. 5 and 6. The Hopf-bifurcation is again found at $q = q_{c3} = 2.15$.

At the critical point $q = q_{c1}$, the order parameter u as a function of the external parameter q is continuous while the its first derivative du/dq is not. No hysteresis is obtained. Thus the L-H transition in Case B is like a second-order phase transition. Finite change in q is required for finite change in u. In Fig. 8, the results where the external parameter is temporally varied are shown in the same way as in Fig. 7. Even though this case corresponds to the second-order transition, we find clear L to H and H to L transitions since certain time lag required to reach the bifurcated stable solution causes the finite difference in q and accordingly sudden changes in (u, k, f). The ELM-like oscillations are also seen for $q > q_{c3} = 2.15$.

Rather generally, the H mode solution undergoes Hopf bifurcation and sheds a limit cycle for input power above a critical level $q \geq q_{c3}$ (here, e.g., q_{c3} (A case) = 1.42 and q_{c3} (B case) = 2.15). In the H-mode state, the presence of the shear flow stabilizes the resistive g or ballooning mode described by reduced resistive MHD equations, which is unstable in the L-mode. The unstable H-mode found in this paper is due to the imbalance between the shear flow generation by the Reynolds stress and the flow damping by the viscosity. Increasing q further allows this limit cycle to grow in amplitude about the unstable H mode. For the current parameter value settings, the limit cycle continues to grow with q until it approaches the planes $k = 0$ and $f = 0$. As is evident from the governing equations (30)–(32), these planes are invariant; they are impermeable to trajectories. The invariant planes give the lower bound to k and f in the limit cycle. The pressure gradient u then increases linearly with time until its amplitude becomes sufficiently large to kick the trajectory away from the $k = 0$ plane. This in turn ejects the trajectory from the plane $f = 0$, then nonlinear feedback forces u to decrease and the trajectory to return to the invariant planes. The time series of u then takes on the appearance of a sawtooth, and the time series for k and f that

of regular pulses.

We add some remarks on the q-dependence of the frequency and amplitude of the limit cycle. The linear growth rate and frequency for the unstable H-mode are calculated from (44) and (45). Near the critical point $q = q_{c3}$, the linear growth rate and frequency increase with q as $\gamma_l = \mathrm{Real}(\lambda) = C_\gamma(q - q_{c3})$ and $\omega_l = \mathrm{Imag}(\lambda) = \omega_{c3} + C_\omega(q - q_{c3})$ where C_γ, C_ω and ω_{c3} are positive constants and given as $C_\gamma = 0.125$, $C_\omega = 0.448$ and $\omega_{c3} = 1.966$ for Case A. For the limit cycle, the finite amplitude nonlinearity should be taken into account. From the Landau theory, the limit cycle amplitude near critical point is supposed to be proportional to the square root of the linear growth rate or $(q - q_{c3})^{1/2}$. In fact, for Case A, we obtain $\Delta k \simeq 6.0(q - q_{c3})^{1/2}$ where $\Delta k \equiv k_{\max} - k_{\min}$ is the difference between the maximum and minimum values of k along the limit cycle. The limit cycle frequency ω is smaller than the linear frequency ω_l due to the finite amplitude and is given as $\omega \simeq \omega_{c3} - 1.75(q - q_{c3})$ near the critical point for Case A. Thus, the oscillation frequency decreases with the input power, and this tendency is consistent with the experimental observations for type III ELMs.[29]

V. Conclusions and Discussion

In this work, we have derived a 3-dimensional state space dynamical model of the L-H dynamics and transitions. The model predicts the temporal evolution of the potential energy $U(t)$ contained in the pressure gradient, the turbulent kinetic energy $K(t)$ and the background shear flow energy $F(t)$. The model is derived from the energy balance equations by modeling the energy transfer and dissipation terms in terms of the three energy variables (U, K, F). The thermal power input P_U into the peripheral region is the external control parameter in our model. Kukharkin *et al.*[23] also proposed an L-H transition model consisting of three ODEs although that model has terms of a different form from those presented here, and especially it does not contain the external parameter corresponding to P_U. If we freeze U, the equations for K and F reduce to the 2-ODE model of the same form as that of

Diamond *et al.*[6]

We have made estimates of the critical conditions required for achieving the H mode for typical tokamak edge parameters There are two conditions that must be satisfied for the H mode to occur. First, the viscous drag (neoclassical or otherwise) controlled by μ must be sufficiently small compared to the edge diffusivity D_L as given by Eq. (24). In practice this requires that the edge ion temperature must be above a certain level (of order $50 - 100\,\mathrm{ev}$). Secondly, with condition (24) satisfied there must be sufficient power ($P_U \rightarrow q$) injected into the edge plasma as given by condition (28). While precise calculations are beyond the scope of the present work, we make the following estimates.

The critical power calculations are made by using Eq. (28) with the composite constant C_T taken as unity to estimate the critical power into the edge plasma as

$$P_{\mathrm{in}} = 4\pi^2 a\, R(3/2)\, \langle \tilde{p}\tilde{v}_x \rangle_c = 6\pi^2 a\, R\, C_T\, D_p |dP_0/dx|$$

where D_p is the effective pressure diffusivity at the edge, respectively. For reference parameters we take $a = 0.3\,\mathrm{m}$, $R = 1.0\,\mathrm{m}$, $D_p = 5.0\,\mathrm{m}^2/\mathrm{s}$. With $L_p = |d\ell n\, P_0/dx|^{-1} = 0.10\,\mathrm{m}$ we get $P_{\mathrm{in}} \simeq 140\,\mathrm{kW}$; and with $L_p = 0.05\,\mathrm{m}$ and $P_0 = 1.0 \times 10^{21}\,\mathrm{eV/m^3}$, we get $P_{\mathrm{in}} \simeq 570\,\mathrm{kW}$ The time scale for the L to H transition decreases with the input power since, from Eq.(40), the growth rate for the unstable L-mode is proportional to $(d(u_L) - m(u_L))$, which increases with q. For the radius of curvature $L_C = 2\,\mathrm{m}$ and $T_i + T_e = 100\,\mathrm{eV}$ we estimate the transition time, when well past the critical power level, to be of order $50\,\mu\mathrm{s}$. These estimates are certainly idealizations due to numerous simplifications. The most important generalization to include may be the coupling through radial diffusion of the local L-H shear-flow transition layer analyzed here to neighboring regions with weak shear flow. This coupling may slow down the time for the L-H transition considerably as well as raising the critical power requirement.

Our dynamical model has the stationary solutions corresponding to the L and H confine-

ment modes. Depending on the value of the external parameter P_U, their stabilities change. The pressure gradient energy U of the stable stationary solution is considered as the order parameter of our system which then yields a function $U = U(P_U)$. We have examined two cases: one is Case A, (first-order phase transition) in which $U(P_U)$ is discontinuous at the transition and the system exhibits the hystersis property. Case A may also be called the hard onset of the H mode. Another Case B (second-order phase transition) in which $U(P_U)$ but dU/dP_U is not discontinuous at the transition. This may also be called the soft onset of the H mode.

The model also predicts the criterion for the loss of stability of the H mode, and the observed Hopf bifurcation from the stable to the unstable H mode gives the attracting limit cycle which behaves like the ELM plasma state. The limit cycle is a relaxation oscillation with intermittent bursts (Fig. 6(d)) of high turbulence levels and associated transport that allow the system to pass through the higher input power P_U values that trigger the ELM state. In the 2-ODE model by Diamond *et al.* where U is treated as an external parameter, we have neither a first-order phase transition nor the unstable H mode. In the L-H transition model by Hinton,[5] the relation between the thermal flux and the temperature gradient similar to the (P_U, U)-curve in Case A is presented. In Hinton's model, the poloidal flow is given from the temperature gradient by the neoclassical theory while the poloidal shear flow effect on the anomalous transport is separately modeled using the argument by Biglari *et al.*[2] and the transport coefficient of drift wave turbulence. However, in our model, the interrelation between the pressure gradient as a turbulence source, the turbulence energy as a cause of anomalous transport and the shear flow as a stabilizer of the turbulence are self-consistently coupled. The coupling is calculated by taking into account energy transfer nonlinearities due to the product of the thermal transport flux and the pressure gradient and due to that of the momentum transport from the Reynolds stress and the shear flow gradient. Because of the abrupt change and the hysteresis property, the first-order-like phase transition seems to

be supported by the experimental results although we found clear transition interval from the temporal evolution of the numerical solution in Case B due to the time lag for reaching to the bifurcated stable point. Figure 5(c) shows an example of the time lag for a case just above the critical power required in Case A and a similar one is found also in Case B. In order to have the functional form of the viscosity for the first-order transition as in Case A, $\nu_{*i} \ll 1$ is required, as mentioned earlier, and therefore low density is preferred.

A corresponding problem in neutral fluids is the onset of large-scale flows in the turbulent Rayleigh-Benard convection at low Prandtl (normalized viscosity) number. A truncated 6-ODE model derived from the 2D partial differential equations is analyzed by Howard and Krishnamurti.[24] They also find a sequence of bifurcations from steady convection states to oscillating states. In addition, they report on a further bifurcation to chaotic solutions associated with heteroclinic orbits. They do not attempt to establish the correspondence of the truncated model with the solutions of the nonlinear partial differential equations.

Recently, Zohm *et al.*[25] extended the model by Itoh *et al.*[26] to investigate the grassy ELM[27] in the dithering H mode. The dithering H mode can be regarded as oscillations between the L and H mode states. On the other hand, the oscillations in the unstable H mode were found to have a different nature, and may correspond to another type of ELM, such as type III ELM[28, 29, 30] since its amplitude and frequency was found to be changeable, depending on the condition. The resistive pressure-gradient-driven fluctuations are considered to be correlated with it. Note that the criterion (46) for the unstable H mode depends on the effective viscosity driven by the pressure gradient. The models by Itoh *et al.* and by Zohm *et al.* are based on the ion orbit loss mechanism and also take into account the temporal and spatial dependencies. There the grassy ELM in the dithering H mode is reproduced by considering the spatial diffusion of the density and the electric field (Zohm *et al.* include the temperature as well). In our model, the spatial structures are not considered and inclusion of them into our model remains an important task, since the

shear flow width may be related to the diffusivity of the electric field.[25, 26, 31] However the significant difference between their models and ours is that we include the turbulence energy K as a basic variable and consider self-consistently the interaction between the turbulence and shear flow. Thus in our model the change in anomalous transports in the L and H modes is naturally derived from the temporal evolution of K, while in theirs the turbulence variable is not explicitly treated, and only ad hoc expressions of the anomalous particle and thermal diffusivities in terms of the electric field are used.

There remain some issues for the investigation in our model, such as the functional forms of the diffusivity and viscosity as well as the values of the dimensionless numerical constants. Here we have explained the general behavior of the L-H transition dynamics within the context of a self-consistent turbulent transport model. However, further investigation on the model is necessary especially on the viscosity function since its form affects the critical point and the type of the transition as well as the occurrence of the ELM-like instability. As an extension of our model, the macroscopic spatial structures of the three variables should be described by the partial differential equations (PDE model) taking into account their transport. This spatial extension is required to address the issue of the nonlocal versus local nature of the L-H transition. In our previous work,[7] the shear flow generation by the Reynolds stress divergence from the resistive g mode is confirmed by the single-helicity nonlinear simulation although in that simulation the energy input is modeled by fixed pressure gradient (which is a conventional technique). In such simulations, we observed that the reduced 2-ODE model describes well the qualitative behavior of the solutions. Comparison between our 3-ODE model with numerical turbulence simulation, which includes the energy input as an external parameter and allowing the self-consistent variation of the pressure gradient, is an interesting research problem for future studies.

Acknowledgments

One of the authors (HS) thanks Prof. M. Okamoto for his encouragements of this work and Prof. M. Wakatani for useful discussions. Part of the work was done during the visit of HS at the Institut für Theoretische Physik I in the Heinrich-Heine-Universität Düsseldorf, and he wishes to thank Prof. Spatschek for helpful discussions and for providing the productive environment for the numerical calculations. The other author (WH) thanks Dr. N. Balmforth for useful discussions. The work was partially supported by the National Institute for Fusion Sciences and the U.S. Department of Energy contract #DE-FG05-80ET-53088.

References

[1]S.-I. Itoh and K. Itoh, Phys. Rev. Lett. **60**, 2276 (1988).

[2]H. Biglari, P.H. Diamond, and P.W. Terry, Phys. Fluids B **2**, 1 (1990).

[3]K.C. Shaing and E.C. Crume, Jr., Phys. Rev. Lett. **63**, 2369 (1989); K.C. Shaing, E.C. Crume, Jr., and W.A. Houlberg, Phys. Fluids B **2**, 1492 (1990).

[4]A.B. Hassam, T.M. Antonsen, Jr., J.F. Drake, and C.S. Liu, Phys. Rev. Lett. **66**, 309 (1991).

[5]F.L. Hinton, Phys. Fluids B **3**, 696 (1991).

[6]P.H. Diamond, V. Shapiro, V. Shevchenko, Y.-B. Kim, M.N. Rosenbluth, B.A. Carreras, K. Sidikman, V.E. Lynch, L. Garcia, P.W. Terry, and R.Z. Sagdeev, in *Plasma Physics and Controlled Nuclear Fusion Research, 1992*, Proceedings of the 14th International Conference, Würzburg (International Atomic Energy Agency, Vienna, 1993), p. 97.

[7]H. Sugama and W. Horton, Phys. Plasmas **1**, 345 (1994).

[8]H.P. Furth, J. Killeen, and M.N. Rosenbluth, Phys. Fluids **6**, 459 (1963).

[9]S. Hamaguchi, Phys. Fluids B **1**, 1416 (1989).

[10]B.A. Carreras, L. Garcia, and P.H. Diamond, Phys. Fluids **30**, 1388 (1987).

[11]H. Sugama and M. Wakatani, J. Phys. Soc. Jpn. **57**, 2010 (1988).

[12]H. Sugama and M. Wakatani, Phys. Fluids B **3**, 1110 (1991).

[13]H. Sugama, M. Wakatani, and A. Hasegawa, Phys. Fluids **31**, 1601 (1988).

[14]P.H. Diamond and Y.-B. Kim, Phys. Fluids B **3**, 1626 (1991).

[15]B.A. Carreras, V.E. Lynch, and L. Garcia, Phys. Fluids B **3**, 1438 (1991).

[16]J.F. Drake, J.M. Finn, P. Guzdar, V. Shapiro, V. Shevchenko, F. Waelbroeck, A.B. Hassam, C.S. Liu, and R. Sagdeev, Phys. Fluids B **4**, 488 (1992).

[17]X.N. Su, P.N. Yushmanov, J.Q. Dong, and W. Horton, Phys. Plasmas **1**, 1905 (1994).

[18]J.-N. Leboeuf, L.A. Charlton, and B.A. Carreras, Phys. Fluids B **5**, 2959 (1993).

[19]H.R. Strauss, Phys. Plasmas **22**, 733 (1980).

[20]H. Sugama, M. Okamoto, and M. Wakatani, in *Plasma Physics and Controlled Nuclear Fusion Research, 1992*, Proceedings of the 14th International Conference, Würzburg (International Atomic Energy Agency, Vienna, 1993).

[21]J. Connor, Plasma Phys. Contr. Fusion **30**, 619 (1988).

[22]S.P. Hirshman, Phys. Fluids **21**, 224 (1978).

[23]M.N. Kukharkin, M.V. Osipenko, O.P. Pogutse, and V.M. Gribkov, in *Plasma Physics and Controlled Nuclear Fusion Research, 1992*, Proceedings of the 14th International Conference, Würzburg (International Atomic Energy Agency, Vienna, 1993).

[24]L.N. Howard and R. Krishnamurti, J. Fluid Mech. **170**, 385 (1986).

[25]H. Zohm, ASDEX-Upgrade Team and NI and ICRH Group, Phys. Rev. Lett. **72**, 222 (1994).

[26]S.-I. Itoh, K. Itoh, A. Fukuyama, Y. Miura, and JFT-2M Group, Phys. Rev. Lett. **67**, 2485 (1991).

[27]ASDEX Team, Nucl. Fusion **29**, 1959 (1989).

[28]R.J. Groebner, Phys. Fluids B **5**, 2343 (1993).

[29]DIII-D Team, *Plasma Physics and Controlled Nuclear Fusion Research, 1990* (International Atomic Energy Agency, Vienna, 1991), Vol. I, p. 69.

[30]H. Zohm, F. Wagner, M. Endler, J. Gernhardt, E. Holzhauer, W. Kerner, and V. Mertens, Nucl. Fusion **32**, 489 (1992).

[31]P.N. Yushmanov, J.Q. Dong, W. Horton, X.-N. Su, and S.I. Krasheninnikov, Phys. Plasmas **1**, 1583 (1994).

Figure Captions

1. The functional forms of $UD_L(U)$ and $U\mu(U)$. $UD_L(U)$ is assumed to be a monotonically increasing function of U. (a) $U\mu(U)$ has a minimum value at $U = U_{c2}(> U_{c1})$. For $P_{c2} < P_U < P_{c1}$, there are three stationary solutions, i.e., U_L, U_{H-} and U_{H+}; (b) $U\mu(U)$ is a monotonically increasing function of U. For $P_U > P_{c1}$, there exist the L and H mode solutions, which are denoted by U_L and U_H, respectively.

2. The stationary solutions plotted in the (u, q)-plane. The solid and dashed curves denote the stable and unstable stationary solutions, respectively. The expressions for $d(u)$ and $m(u)$ are given in Eqs. (47) and (48); (a) and (b) correspond to Case A and Case B, respectively. Arrows in (a) represent the first-order phase transitions showing the hysteresis property.

3. Case A: numerical solution of Eqs. (30)–(32) for $q = 0.8(< q_{c1})$ and $(u, k, f)_{\tau=0} = (0.3, 0.2, 0.1)$. The stable L mode solution is given by $(u_L, k_L, f_L) = (0.89, 0.85, 0)$. (a) The trajectory in the (u, k, f) phase space. (b) The projection of the trajectory onto the (k, f)-plane. (c) The temporal dependence of (u, k, f).

4. Case A: numerical solutions of Eqs. (30)–(32) for $q = 0.9(q_{c2} < q < q_{c1})$. Two different initial conditions $(u, k, f)_{\tau=0} = (1.5, 0.2, 0.08)$ and $(u, k, f)_{\tau=0} = (1.5, 0.2, 0.1)$ are used. There are two stable stationary solutions given by $(u_L, k_L, f_L) = (0.95, 0.92, 0)$ and $(u_{H+}, k_{H+}, f_{H+}) = (2.39, 0.58, 0.40)$, and one unstable stationary solution given by $(u_{H-}, k_{H-}, f_{H-}) = (1.41, 0.76, 0.15)$. (a) The two trajectories in the (u, k, f) phase space starting from $(u, k, f)_{\tau=0} = (1.5, 0.2, 0.08)$ and from $(u, k, f)_{\tau=0} = (1.5, 0.2, 0.1)$. (b) The projection of the two trajectories onto the (k, f)-plane. (c) The temporal dependence of (u, k, f) for $(u, k, f)_{\tau=0} = (1.5, 0.2, 0.08)$. (d) The temporal dependence of (u, k, f) for $(u, k, f)_{\tau=0} = (1.5, 0.2, 0.1)$.

5. Case A: numerical solutions of Eqs. (30)–(32) for $q = 1.05 (q_{c1} < q < q_{c3})$ and $(u, k, f)_{\tau=0} = (0.3, 0.2, 0.1)$. The unstable L mode solution and the stable H mode solution are given by $(u_L, k_L, f_L) = (1.02, 1.04, 0)$ and $(u_H, k_H, f_H) = (3.23, 0.58, 0.58)$, respectively. (a) The trajectory in the (u, k, f) phase space. (b) The projection of the trajectory onto the (k, f)-plane. (c) The temporal dependence of (u, k, f).

6. Case A: numerical solutions of Eqs. (30)–(32) for $q = 1.6 (> q_{c3})$ and $(u, k, f)_{\tau=0} = (0.3, 0.2, 0.1)$. The unstable L mode solution and the unstable H mode solution are given by $(u_L, k_L, f_L) = (1.26, 1.42, 0)$ and $(u_H, k_H, f_H) = (4.83, 0.73, 0.90)$, respectively. (a) The trajectory in the (u, k, f) phase space for $0 \leq \tau \leq 20$ and for the limit cycle. (b) The projection of the trajectory onto the (k, f)-plane for $0 \leq \tau \leq 20$ and for the limit cycle. (c) The temporal dependence of (u, k, f) for $0 \leq \tau \leq 20$. (d) The temporal dependence of (u, k, f) for the limit cycle.

7. Case A: numerical solutions of Eqs. (30)–(32) where the external parameter q is temporally varied. The initial condition is given by $(u, k, f)_{\tau=0} = (0.4, 0.4, 0.4)$. (a) The external parameter $q = q(\tau)$ as a function of time. The three horizontal lines correpond to $q = q_{c1} (= 1)$, $q = q_{c2} (= 0.87)$ and $q = q_{c3} (= 1.42)$. (b) The temporal dependence of (u, k, f). (c) The trajectory in the (u, k, f) phase space. (d) The projection of the trajectory onto the (k, f)-plane.

8. Case B: numerical solution of Eqs. (30)–(32) where the external parameter q is temporally varied. The initial condition is given by $(u, k, f)_{\tau=0} = (0.3, 0.2, 0.1)$. (a) The external parameter $q = q(\tau)$ as a function of time. The two horizontal lines correpond to $q = q_{c1} (= 1)$ and $q = q_{c3} (= 2.15)$. (b) The temporal dependence of (u, k, f).

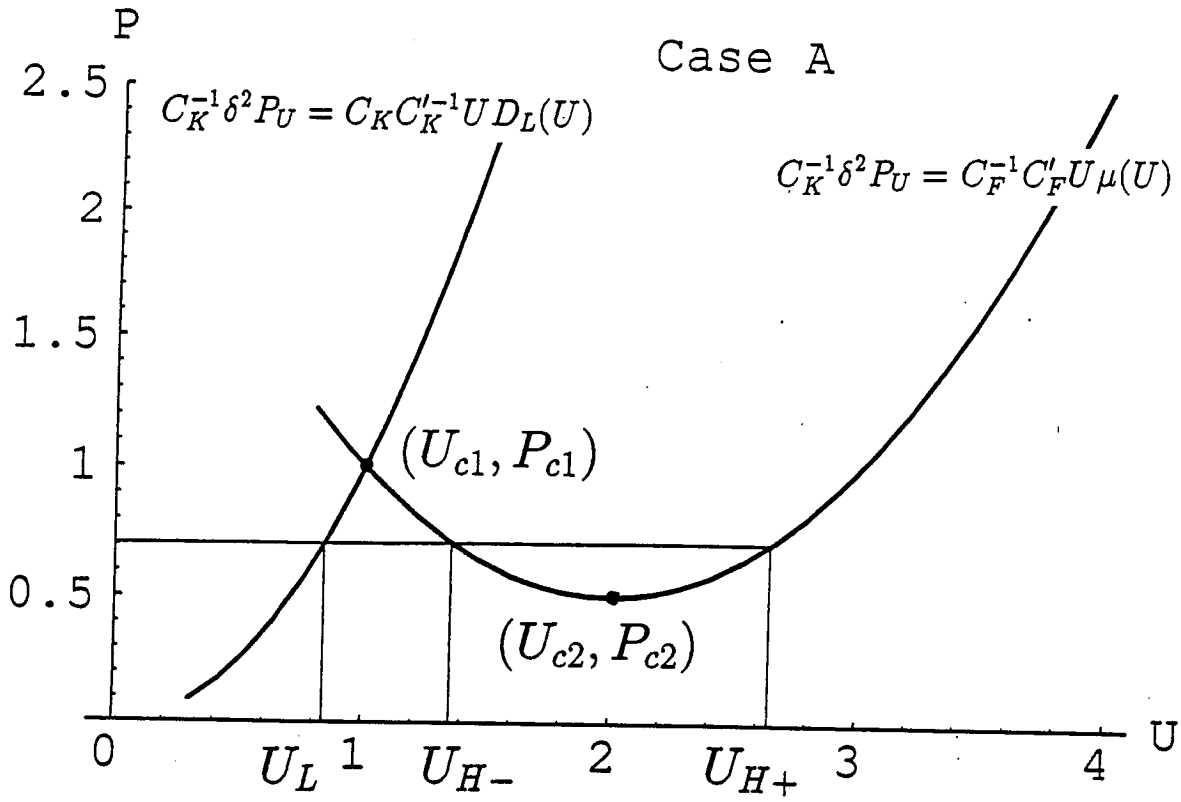
Case A
P
2.5
2
1.5
1
0.5
$C_K^{-1}\delta^2 P_U = C_K C_K'^{-1} U D_L(U)$
$C_K^{-1}\delta^2 P_U = C_F^{-1} C_F' U \mu(U)$
(U_{c1}, P_{c1})
(U_{c2}, P_{c2})
0
U_L
1
U_{H-}
2
U_{H+}
3
4
U

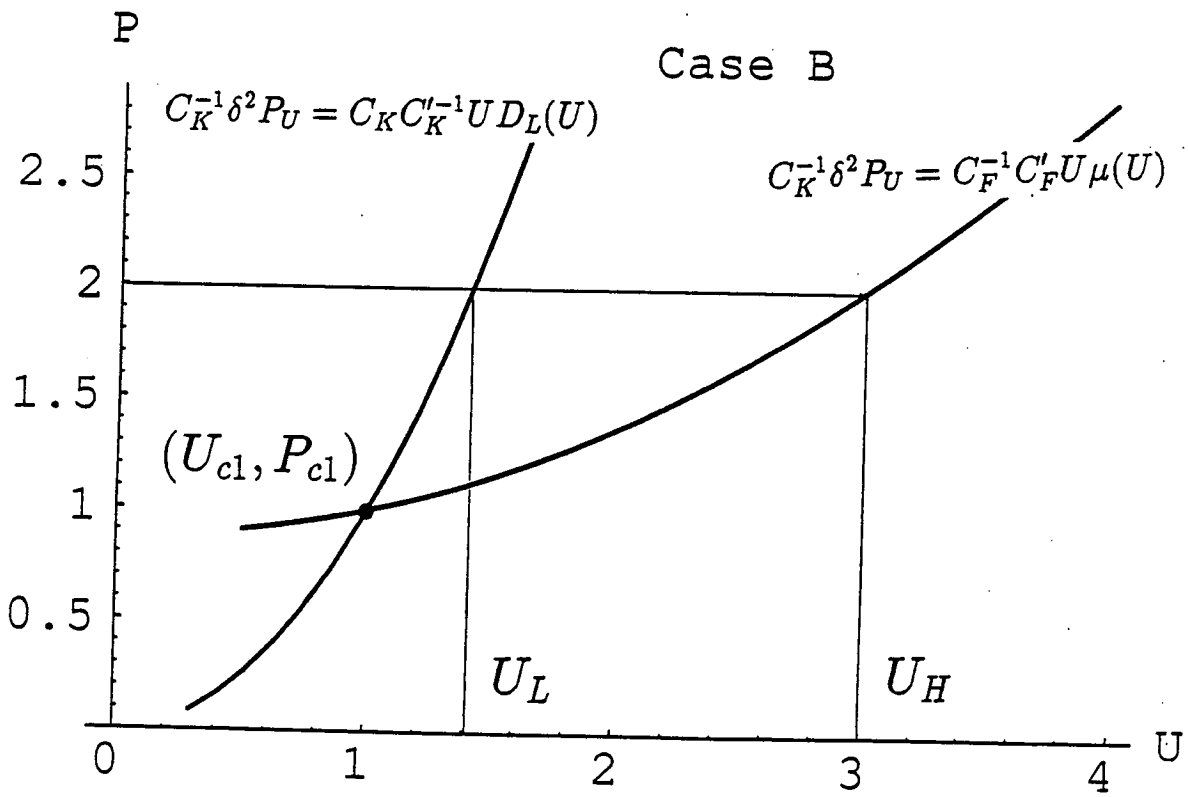
Case B
P
2.5
2
1.5
1
0.5
$C_K^{-1}\delta^2 P_U = C_K C_K'^{-1} U D_L(U)$
$C_K^{-1}\delta^2 P_U = C_F^{-1} C_F' U \mu(U)$
(U_{c1}, P_{c1})
U_L
U_H
0
1
2
3
4
U

Fig.1

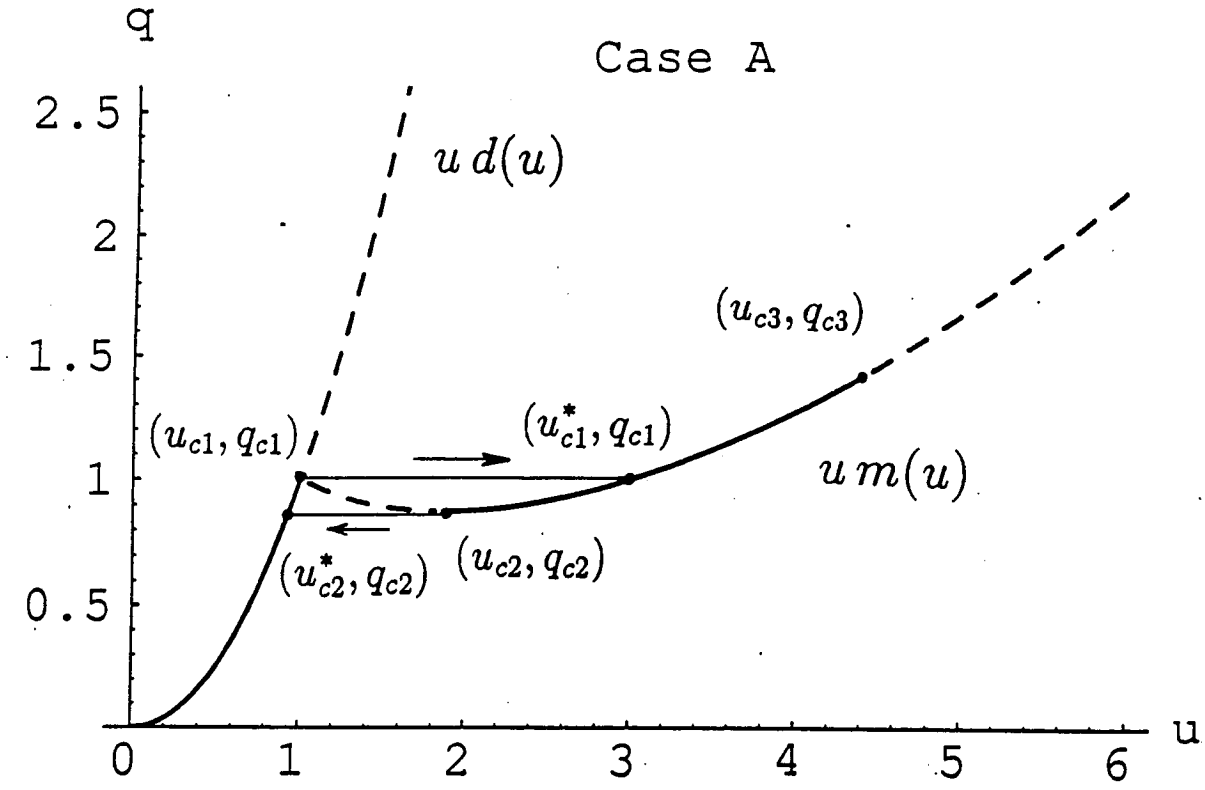
q
Case A
2.5
2
1.5
1
0.5
$u\,d(u)$
(u_{c3}, q_{c3})
(u_{c1}, q_{c1})
(u^*_{c1}, q_{c1})
$u\,m(u)$
(u^*_{c2}, q_{c2})
(u_{c2}, q_{c2})
0
1
2
3
4
5
6
u

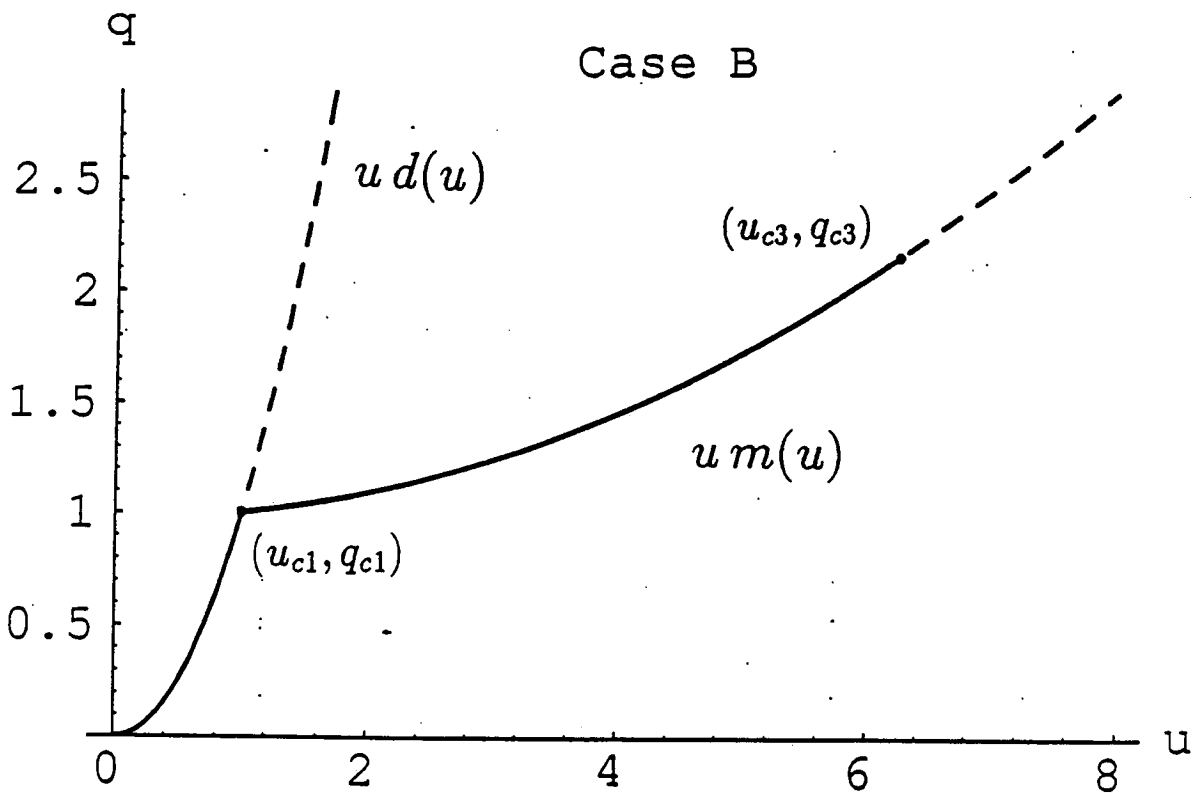
q
Case B
2.5
2
1.5
1
0.5
$u\,d(u)$
(u_{c3}, q_{c3})
$u\,m(u)$
(u_{c1}, q_{c1})
0
2
4
6
8
u

Fig.2

Fig.3(a)

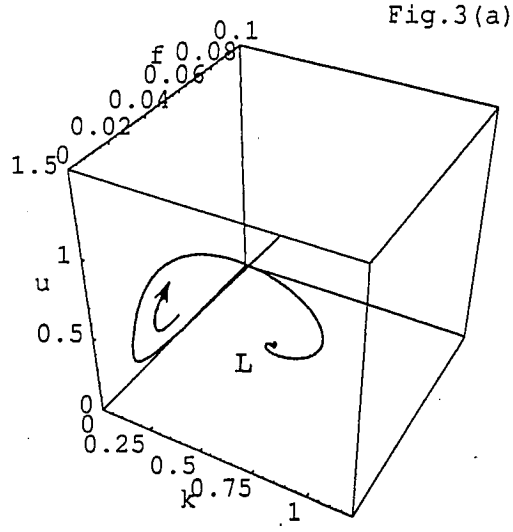

Fig.3(b)

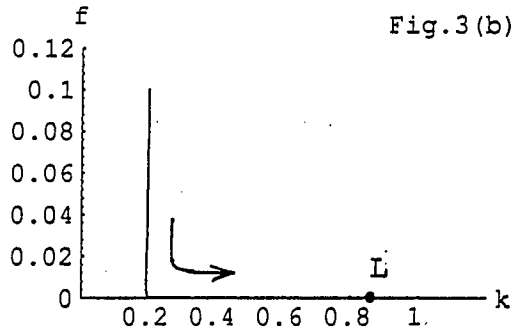

Fig.3(c)

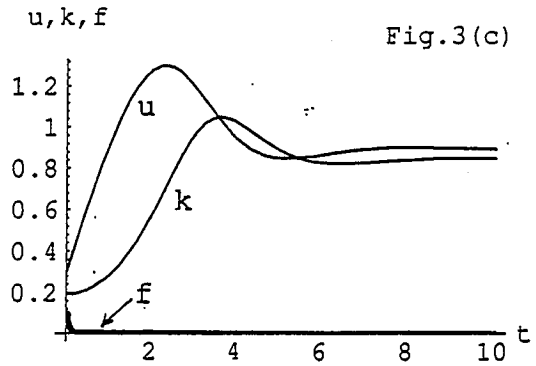

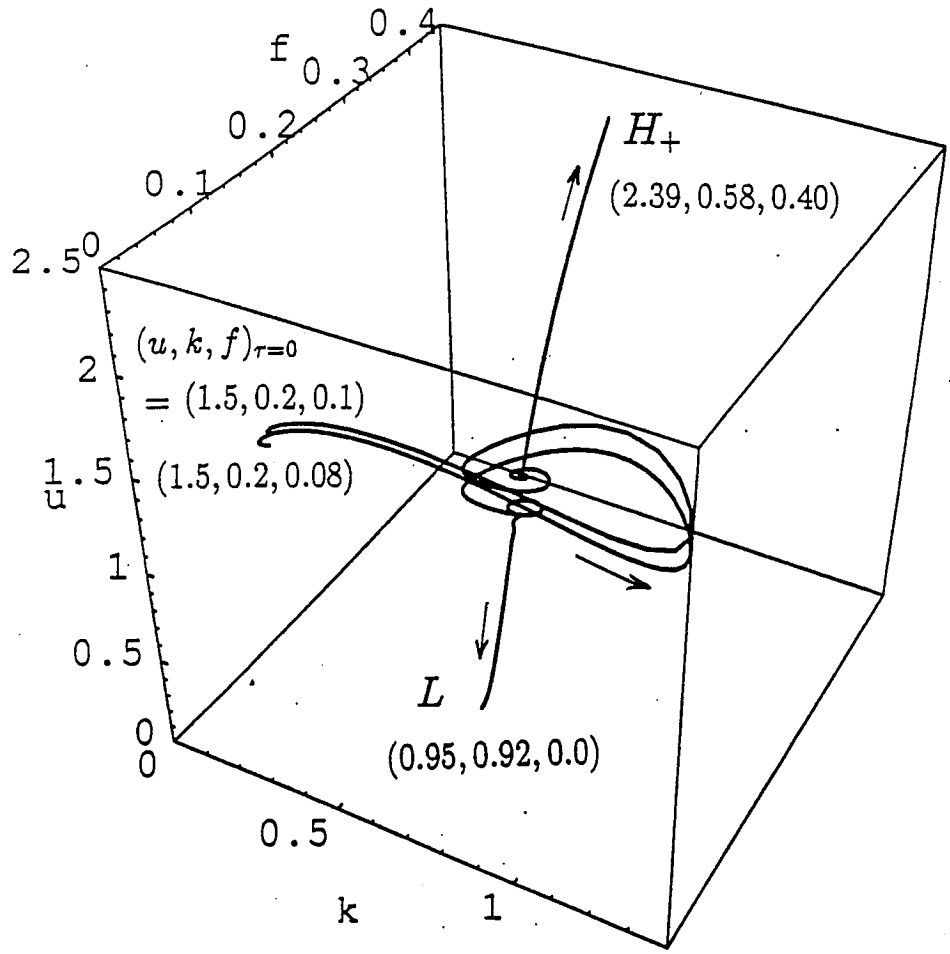
f
0.4
0.3
0.2
0.1
0
2.5
2
1.5
1
0.5
0
u
0
0.5
1
k
H_+
(2.39, 0.58, 0.40)
$(u, k, f)_{\tau=0}$
$= (1.5, 0.2, 0.1)$
(1.5, 0.2, 0.08)
L
(0.95, 0.92, 0.0)

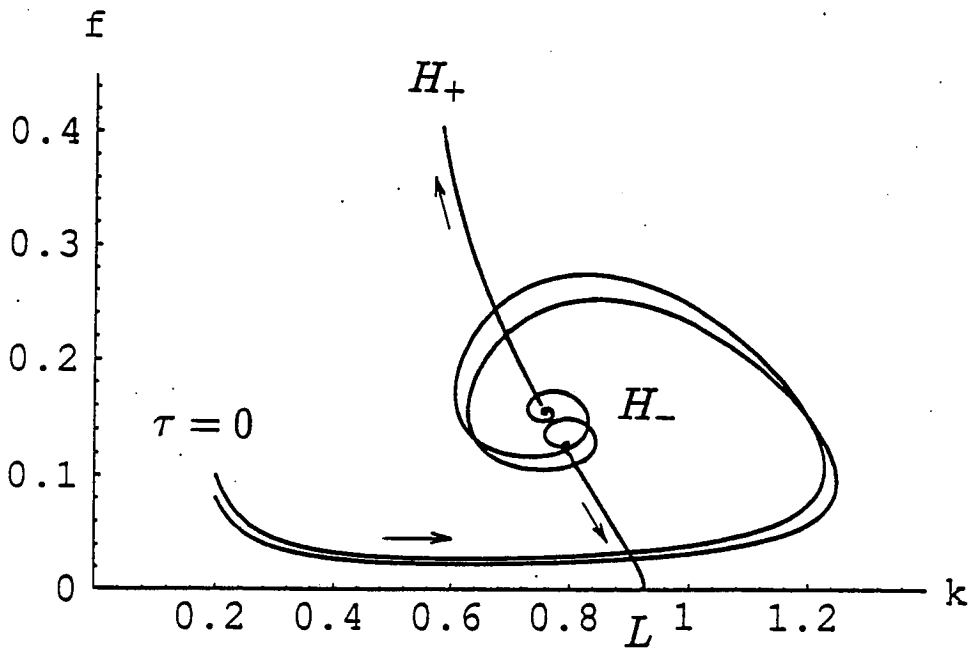
f
0.4
0.3
0.2
0.1
0
0.2
0.4
0.6
0.8
1
1.2
k
H_+
H_-
$\tau = 0$
L

Fig.4 (a), (b)

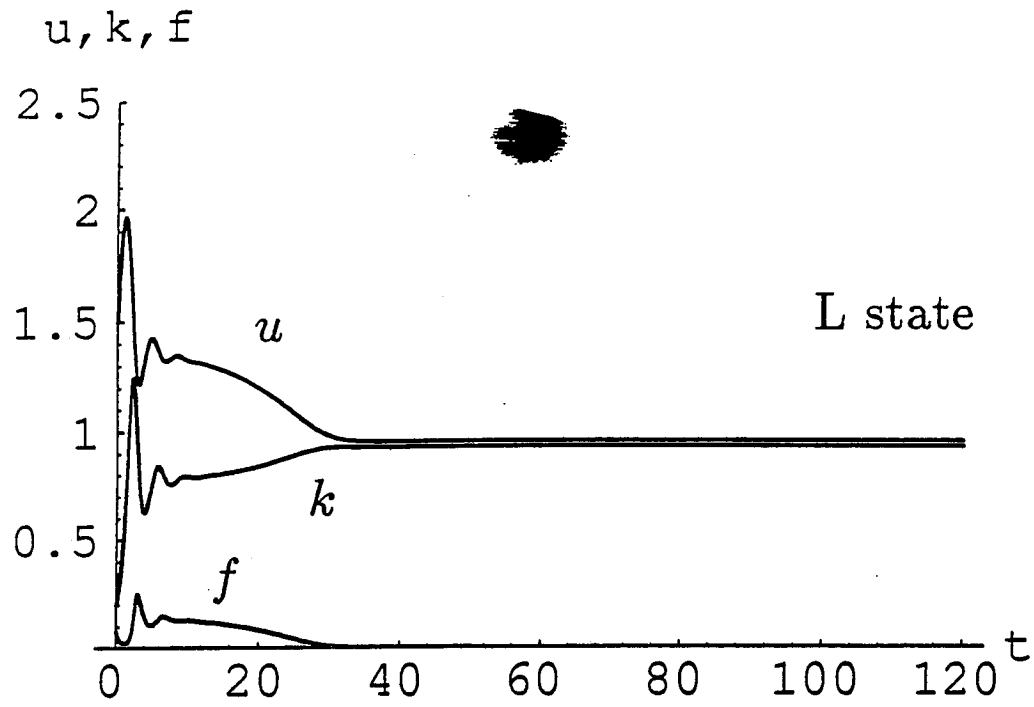
u, k, f
2.5
2
1.5
1
0.5
u
k
f
L state
0
20
40
60
80
100
120
t

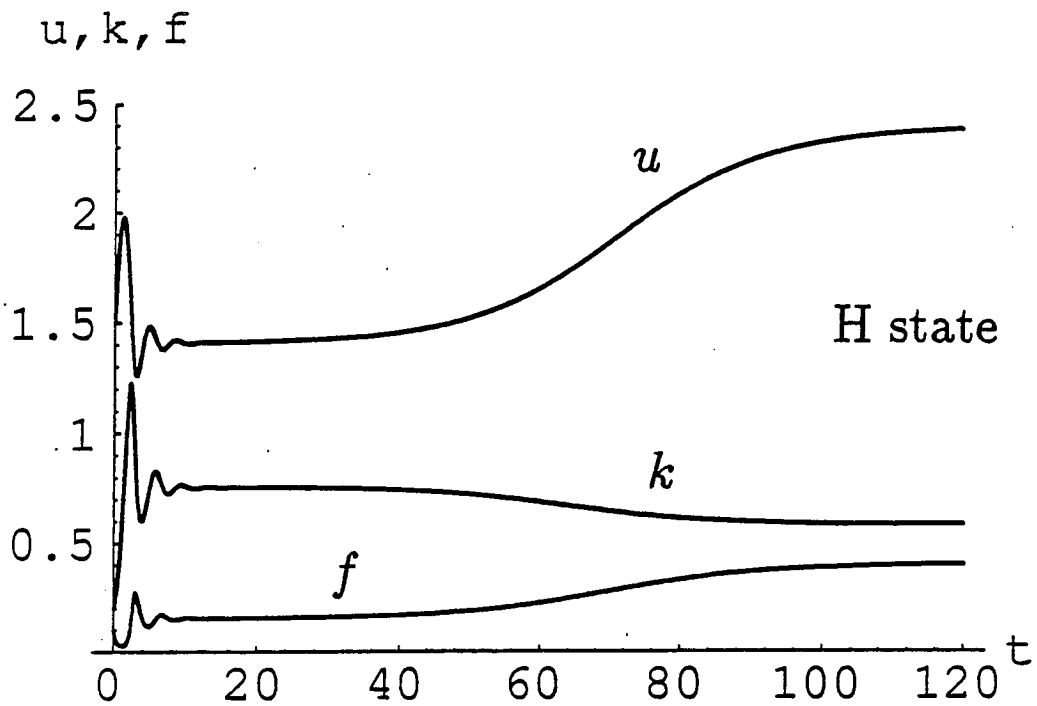
u, k, f
2.5
2
1.5
1
0.5
u
k
f
H state
0
20
40
60
80
100
120
t

Fig.4 (c), (d)

Fig.5(a)

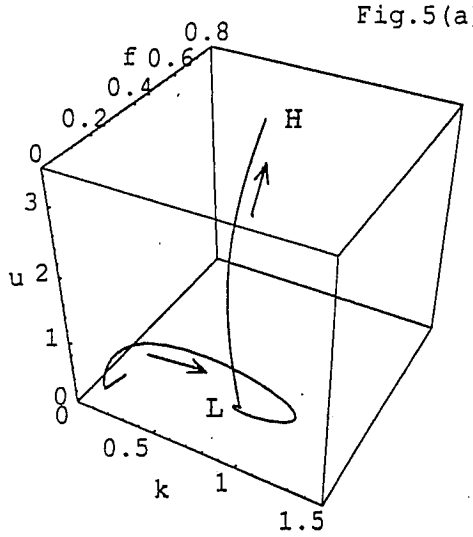

Fig.5(b)

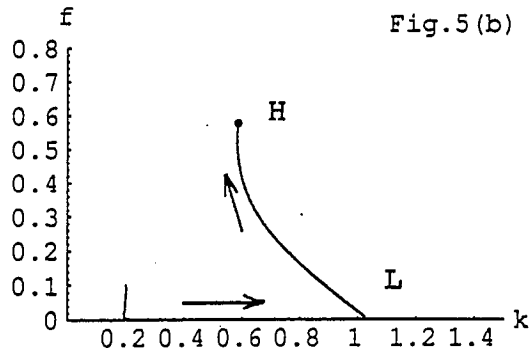

Fig.5(c)

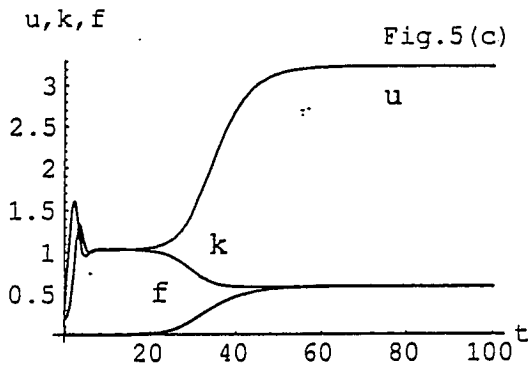

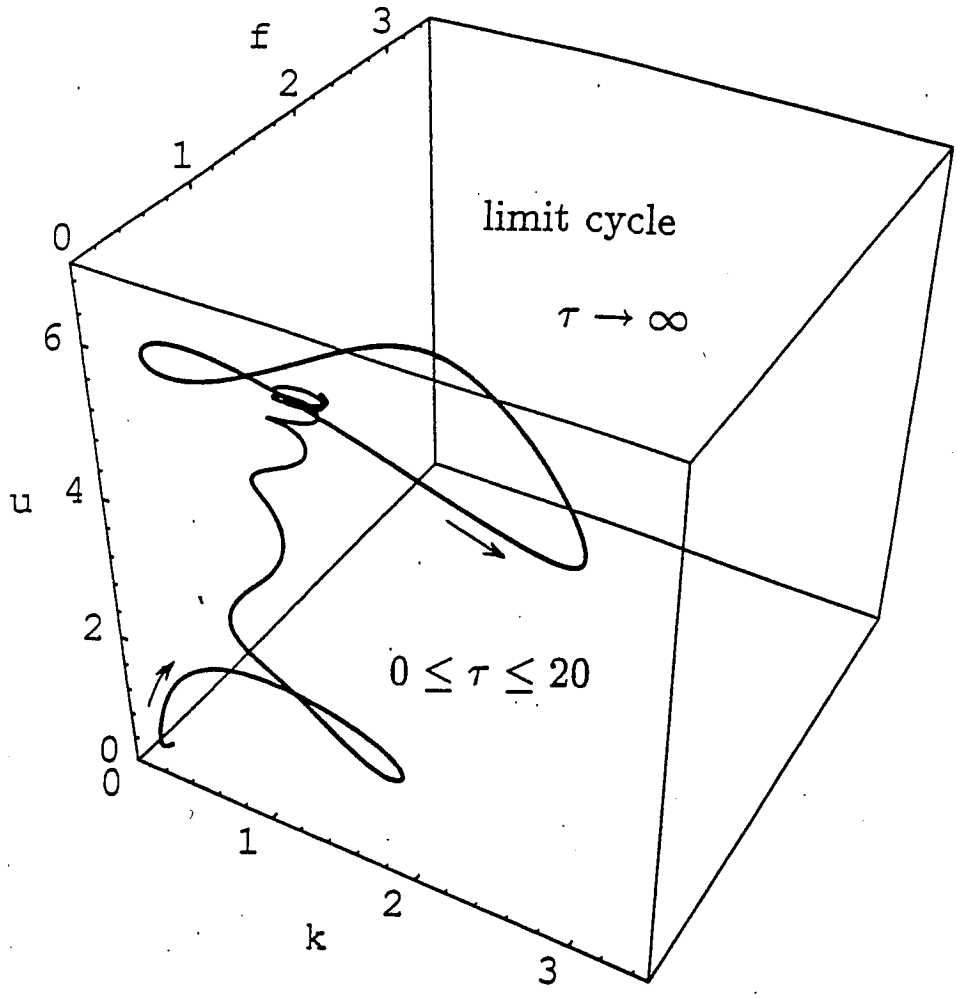
f
3
2
1
0
limit cycle
$\tau \to \infty$
6
u 4
2
0
0
$0 \le \tau \le 20$
1
2
k
3

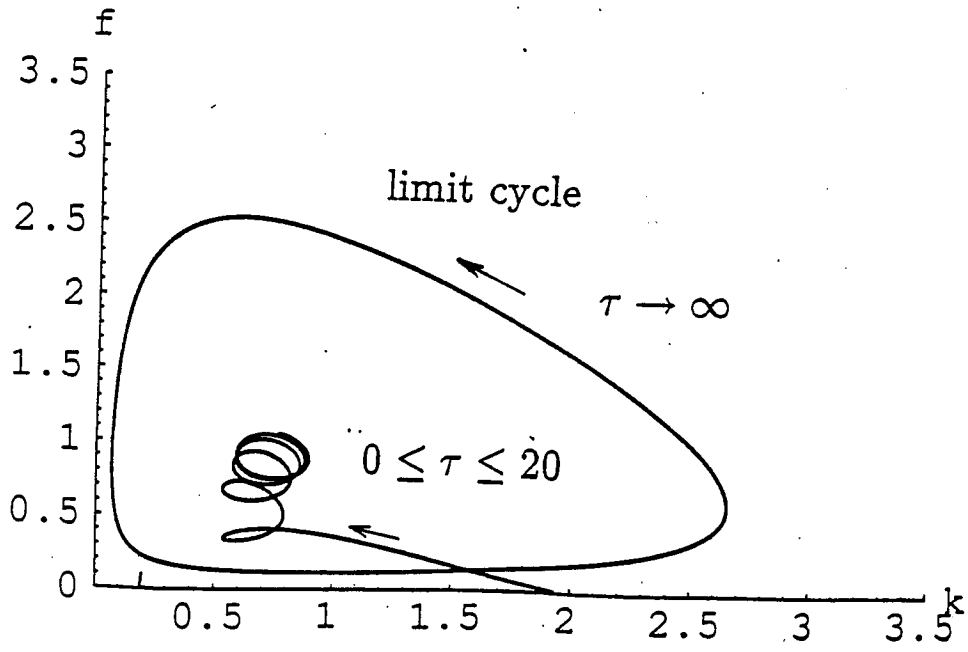
f
3.5
3
2.5
2
1.5
1
0.5
0
limit cycle
$\tau \to \infty$
$0 \le \tau \le 20$
0.5
1
1.5
2
2.5
3
3.5
k

Fig.6 (a), (b)

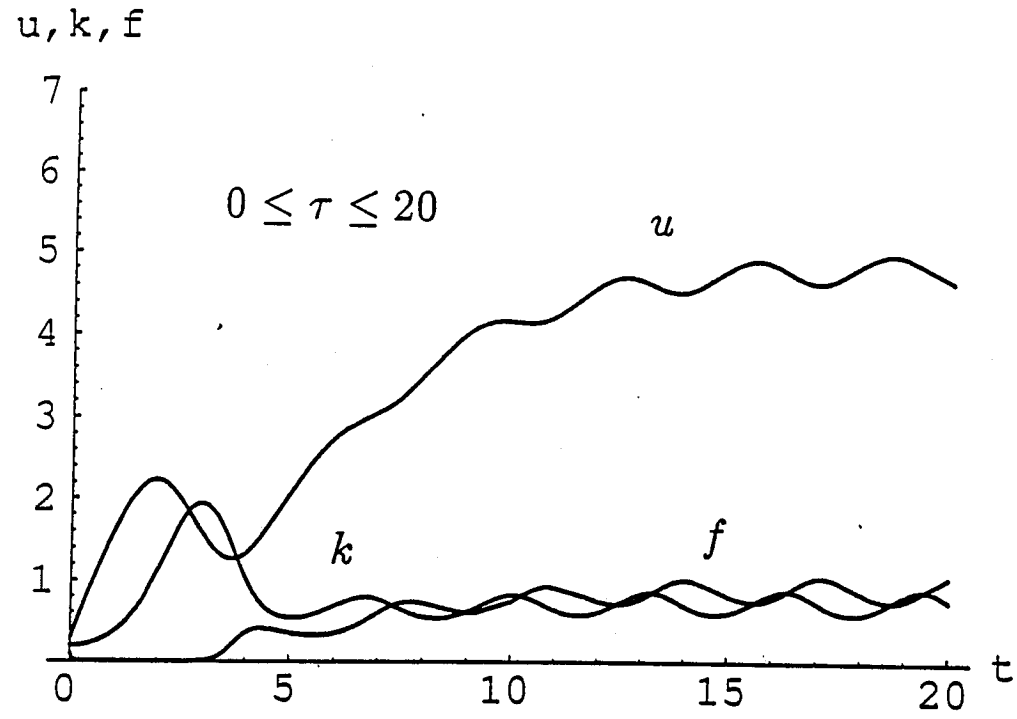
u, k, f
7
6
5
4
3
2
1
$0 \leq \tau \leq 20$
u
k
f
0
5
10
15
20
t

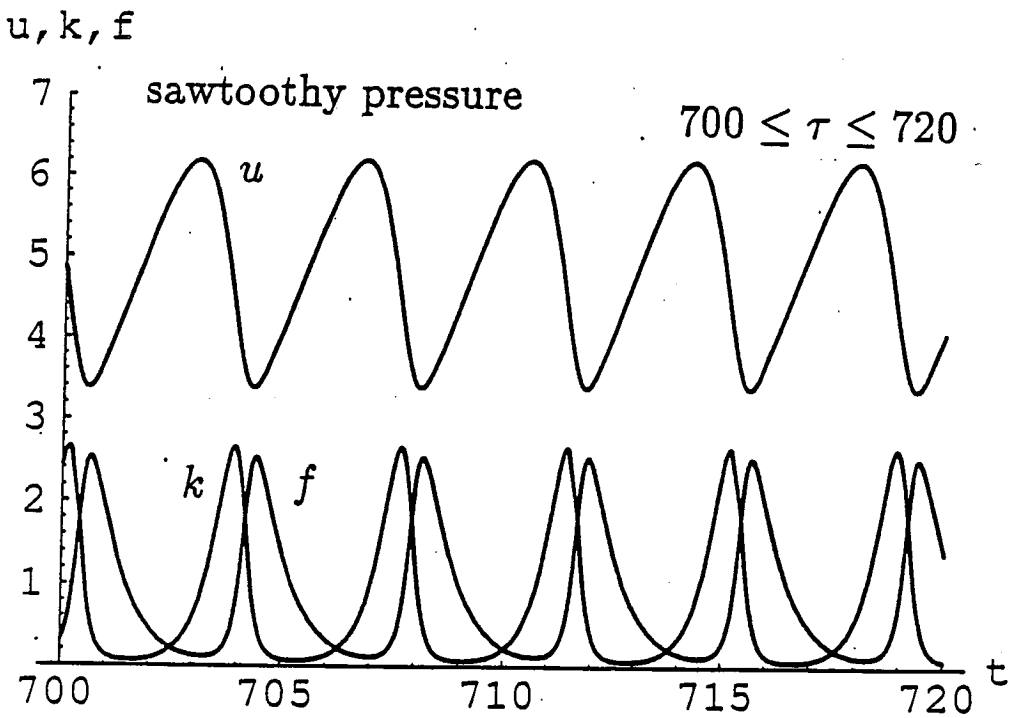
u, k, f
sawtoothy pressure
$700 \leq \tau \leq 720$
7
6
5
4
3
2
1
u
k
f
700
705
710
715
720
t

Fig.6 (c), (d)

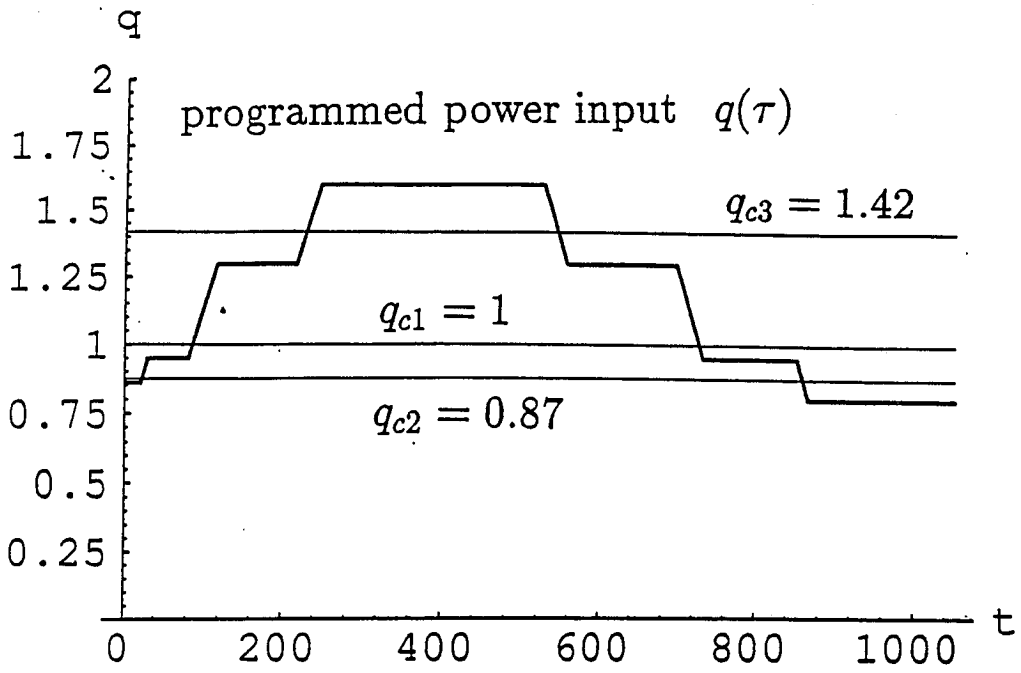
q
programmed power input $q(\tau)$
$q_{c3} = 1.42$
$q_{c1} = 1$
$q_{c2} = 0.87$
2
1.75
1.5
1.25
1
0.75
0.5
0.25
0
200
400
600
800
1000
t

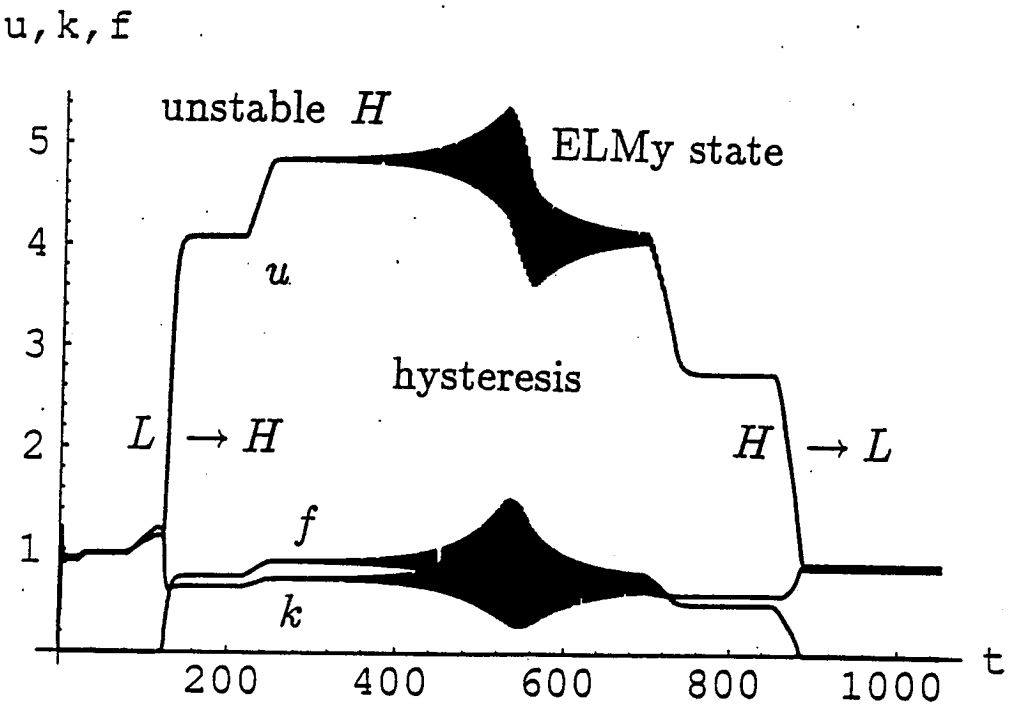
u, k, f
unstable H
ELMy state
u
hysteresis
$L \rightarrow H$
$H \rightarrow L$
f
k
5
4
3
2
1
200
400
600
800
1000
t

Fig.7 (a), (b)

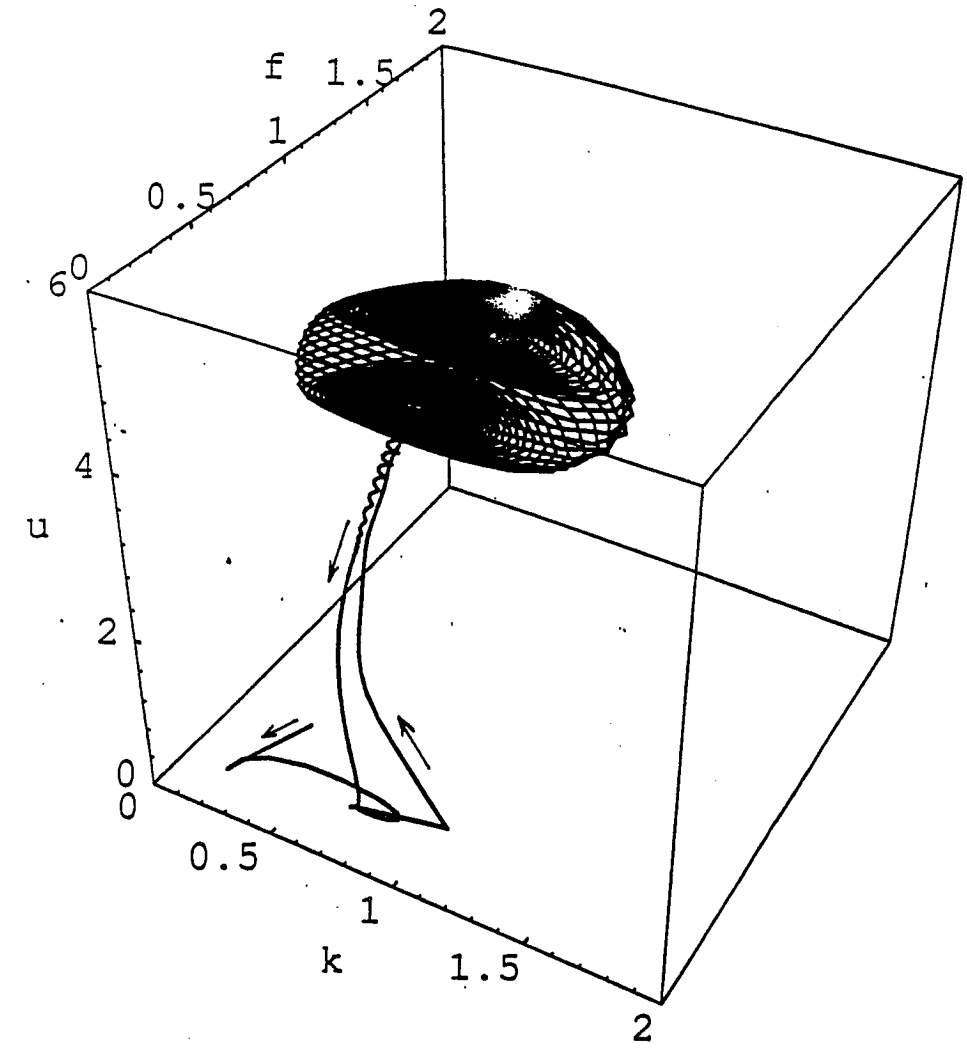
f
2
1.5
1
0.5
0
6
4
u
2
0
0
0.5
1
k
1.5
2

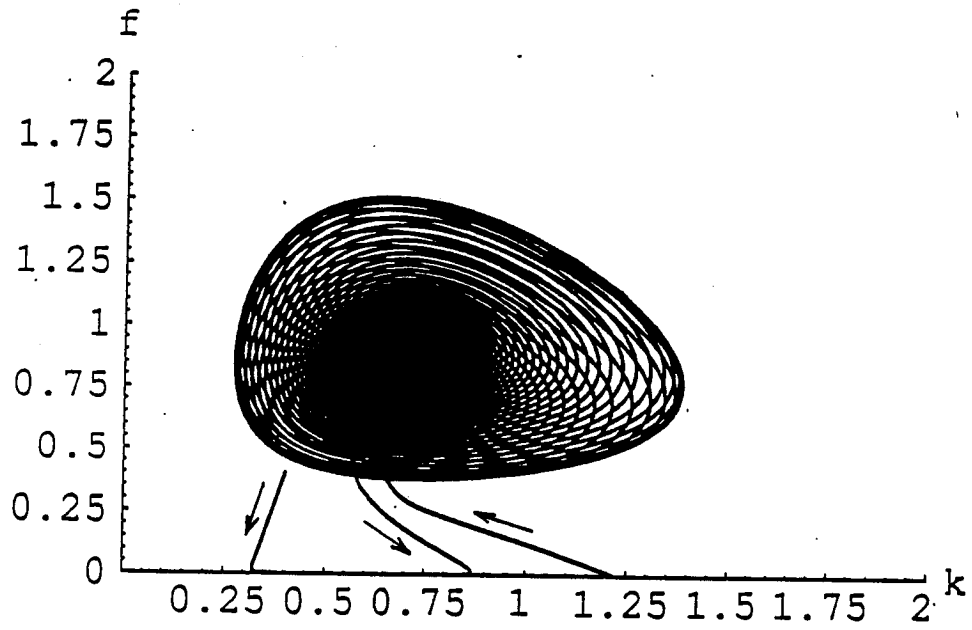
f
2
1.75
1.5
1.25
1
0.75
0.5
0.25
0
0.25 0.5 0.75 1 1.25 1.5 1.75 2
k

Fig.7 (c), (d)

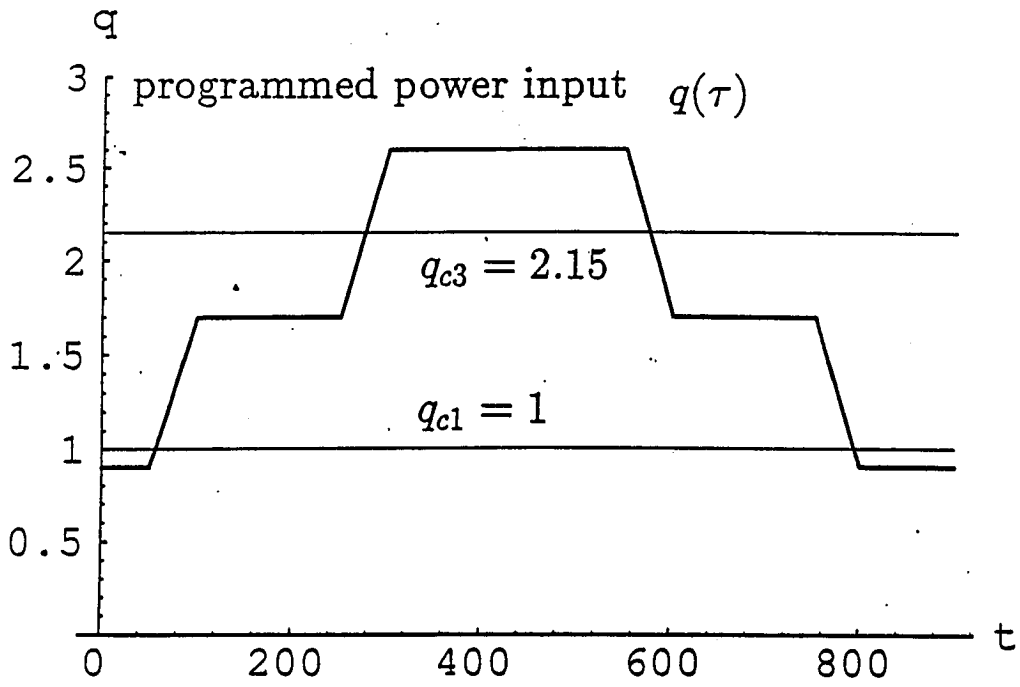
q
programmed power input $q(\tau)$
3
2.5
2
1.5
1
0.5
$q_{c3} = 2.15$
$q_{c1} = 1$
0
200
400
600
800
t

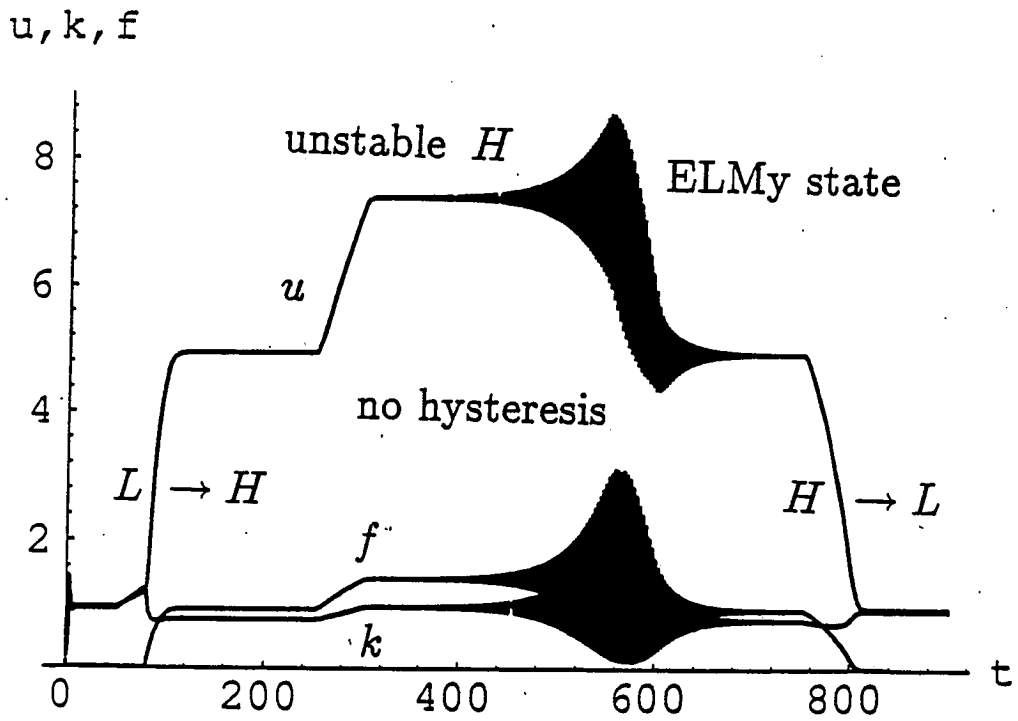
u, k, f
8
6
4
2
unstable H
ELMy state
u
no hysteresis
$L \rightarrow H$
$H \rightarrow L$
f
k
0
200
400
600
800
t

Fig.8